JACS
JOURNAL OF THE AMERICAN CHEMICAL SOCIETY

PERSPECTIVE

pubs.acs.org/JACS

Molecular Design and Ordering Effects in π-Functional Materials for Transistor and Solar Cell Applications

Pierre M. Beaujuge* and Jean M. J. Fréchet*

King Abdullah University of Science and Technology, Thuwal 23955-6900, Saudi Arabia, and College of Chemistry, University of California, Berkeley, California 94720-1460, United States

Supporting Information

ABSTRACT: Organic electronics are broadly anticipated to impact the development of flexible thin-film device technologies. Among these, solution-processable π-conjugated polymers and small molecules are proving particularly promising in field-effect transistors and bulk heterojunction solar cells. This Perspective analyzes some of the most exciting strategies recently suggested in the design and structural organization of π-functional materials for transistor and solar cell applications. Emphasis is placed on the interplay between molecular structure, self-assembling properties, nanoscale and mesoscale ordering, and device efficiency parameters. A critical look at the various approaches used to optimize both materials and device performance is provided to assist in the identification of new directions and further advances.

INTRODUCTION

Over the past decade, substantial progress has been made in understanding the structure−function relationships governing material performance in the field of organic electronics. π-Conjugated polymers and small molecules, which can be solution-processed over large-area substrates, are key components in the development of both mechanically conformable circuit logics and printable light-harvesting technologies. As the performance of organic electronics improves with our understanding of the fundamental requirements for their operation, it is possible to envision their future use as cost-effective thin-film alternatives to conventional silicon-based and other inorganic systems.

With both small molecules and polymers, a first level of control is achieved by modulating the molecular structure of the π-functional system, including the pattern of its solubilizing side chains. The latter is important as it affects not only processing but also self-assembly into ordered domains such as lamellar stacks (Figure 1a) or columns, and the degree of nanoscale (Figure 1b) or mesoscale structural organization attainable in thin films. In turn, the most fundamental material properties of organic electronic systems, such as conjugation length, light absorption, carrier mobilities, exciton dynamics, and processability, can be varied broadly through changes in molecular structure. A second level of control is achieved by optimizing device architecture, material processing conditions, and the strategies that control thin-film ordering. These approaches are proving increasingly critical to uncover the optimal intrinsic capabilities of the various materials examined for a given thin-film device application. For example, interpenetrating networks of electron-donor and electron-acceptor components—called "bulk heterojunctions" (BHJs)—offer larger surface areas for the dissociation of excitons when compared to conventional bilayer heterojunctions (Figure 1c,d). However, multicomponent systems such as BHJs are particularly challenging due to the dominant influence of the overall morphology of the composite. Therefore, in an ideal BHJ, co-continuous donor and acceptor domains with sizes closely related to the diffusion length of excitons should be targeted, while nanoscale ordering within these domains is also an issue. As a result, innovative solution-processing approaches involving low vapor pressure cosolvents or small-molecule additives have proven especially useful by fostering the formation of the most favorable nanoscale morphologies, while improving the microstructural organization in the polymer-rich domains. This strategy is now widely used in the processing of donor−acceptor BHJs relying on fullerene acceptors, for which the highest solar power conversion efficiencies (PCEs) achieved to-date have been reported.

In this Perspective, we analyze some of the most exciting strategies recently suggested for the design and structural organization of π-functional materials for solution-processed organic thin-film transistors (OTFTs) and organic photovoltaic (OPV) devices. Structure−property relationships are explored with an array of polymers and small molecules, emphasizing the impact of simple synthetic modifications on the electronics and the thin-film self-assembly characteristics of these systems. Beyond the key parameters of molecular structure of π-functional materials, the influence of various nanoscale morphologies on charge-carrier dynamics must be well understood in order to improve device efficiencies. As a result, a significant focus of this Perspective is the exploration of ways in which phase separation can be controlled and thin-film microstructural order can be achieved.

Building a fundamental understanding of the structural variables that govern device performance parameters should provide further guidance for the design of new materials and help in optimizing the efficiencies of the promising systems currently being explored for OTFT and OPV applications.

POLYMERS IN TRANSISTORS AND SOLAR CELLS

Of all the semiconducting polymers designed early on for transistor and solar cell applications, including MDMO-PPV and MEH-PPV (**1** and **2**, Chart 1), semicrystalline poly(3-hexylthiophene) (P3HT, **3**, Chart 1) has shown by far the most pronounced organizational capabilities, along with substantial charge-transport properties, thus providing a high degree of flexibility for application in devices. Figure 2 shows the lamellar assembly which dominates the crystalline

Received: August 5, 2011
Published: October 14, 2011

dx.doi.org/10.1021/ja2073643 | J. Am. Chem. Soc. 2011, 133, 20009–20029

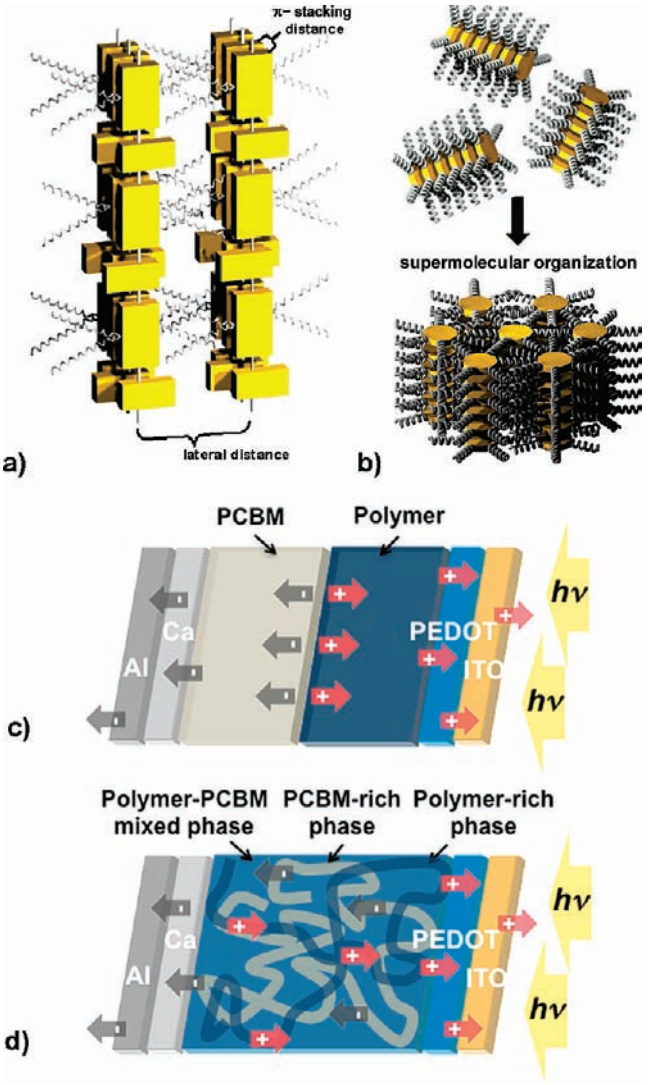

Figure 1. (a) Schematic representation of the π-stacking and lamellar organizations of a representative alkyl-substituted π-conjugated polymer. Reproduced with permission from ref 1. Copyright 2007 American Chemical Society. (b) Illustration of the supramolecular self-assembly of alkyl-substituted polycyclic aromatic hydrocarbon discotics. Reproduced with permission from ref 2. Copyright 2007 American Chemical Society. Charge dissociation and collection (c) in a bilayer heterojunction solar cell device of polymer donor and PCBM acceptor, and (d) in a bulk heterojunction, providing a greater surface area for the dissociation of excitons.

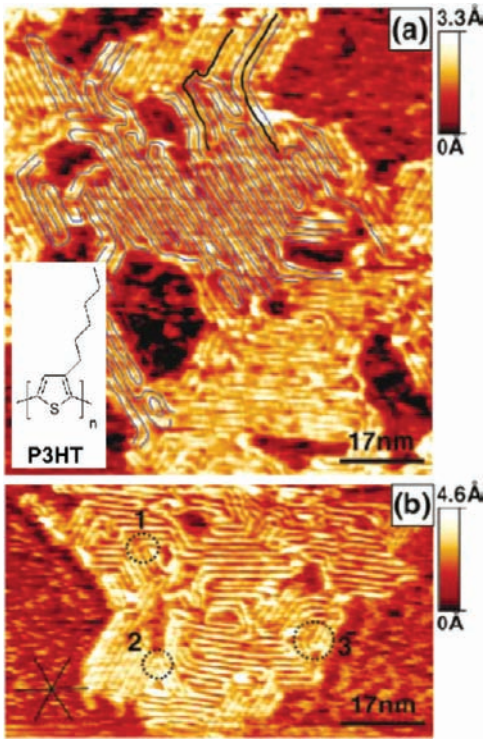

Figure 2. (a) Magnified scanning tunneling microscopy (STM) image showing the lamellar organization dominating crystalline monodomains of P3HT (**3**) on oriented graphene. The blue lines underline the chain contours. The black lines emphasize examples of chains connecting two different crystalline monodomains. (b) The dotted circles labeled 1, 2, and 3 emphasize 120°, 60°, and 360° folds, respectively. Reproduced with permission from ref 3. Copyright 2003 American Institute of Physics.

monodomains of P3HT on oriented graphene,[3] and provides a good illustration of the level of self-organization attainable in thin films of semicrystalline polymer semiconductors in general. Building from this ability to form highly ordered domains at the nanoscale, P3HT has provided an excellent platform to study relationships between morphology and performance in both OTFTs and OPV devices.[4−10] A recent study[11] of carrier transport at grain boundaries between different orientations of crystallites in directional thin films of P3HT has highlighted the need to learn how to control grain-boundary placement and relative grain orientation in semicrystalline semiconductors.

In the case of P3HT, the highest reported device efficiencies have been achieved with the most regioregular polymer fractions.[12] However, it has also been observed that decreasing the propensity of P3HT and other polythiophene analogues such as poly(quaterthiophene) (PQT, **4**, Chart 1) to crystallize by intentionally disrupting their regioregularity, or, more broadly, by breaking the symmetry of their repeat unit, can also be beneficial.[13] This concept was implemented in BHJ solar cells incorporating the fullerene acceptor [6,6]-phenyl-C61-butyric acid methyl ester ($PC_{61}BM$, **30**, see Chart 2), which demonstrated improved device efficiency[13] and enhanced thermal stability[14,15] when polymer backbone symmetry was reduced. Similarly, the size of the solubilizing side chains was shown to affect the BHJ nanoscale morphology and OPV device performance of poly(3-alkylthiophene)s, the degree of phase separation and carrier balance increasing with increasing side-chain length.[7,8] In another report, the degree of microstructural order in crystalline fibers of the same polymers was shown to improve with increasing side-chain length.[16]

While the effect of molecular weight (MW) on the performance of P3HT has been emphasized in both OPV and OTFT device architectures,[4,17−22] somewhat conflicting experimental results have been reported by different groups, and the reasons for the variations observed as a function of MW remain somewhat ambiguous. For transistors based on regioregular P3HT, mobility and contact resistance have been shown to improve with increasing MW within the range 5.5−11 kDa, and to saturate when MW exceeds 11 kDa.[4,20] These results were correlated to the propensity of P3HT to form nanofibrillar morphologies, whereby the width of the nanofibrils increased with increasing MW. In a separate study, the hole mobilities, estimated by the time-of-flight approach in thin films of highly regioregular P3HT, were shown to (i) remain relatively

Chart 1

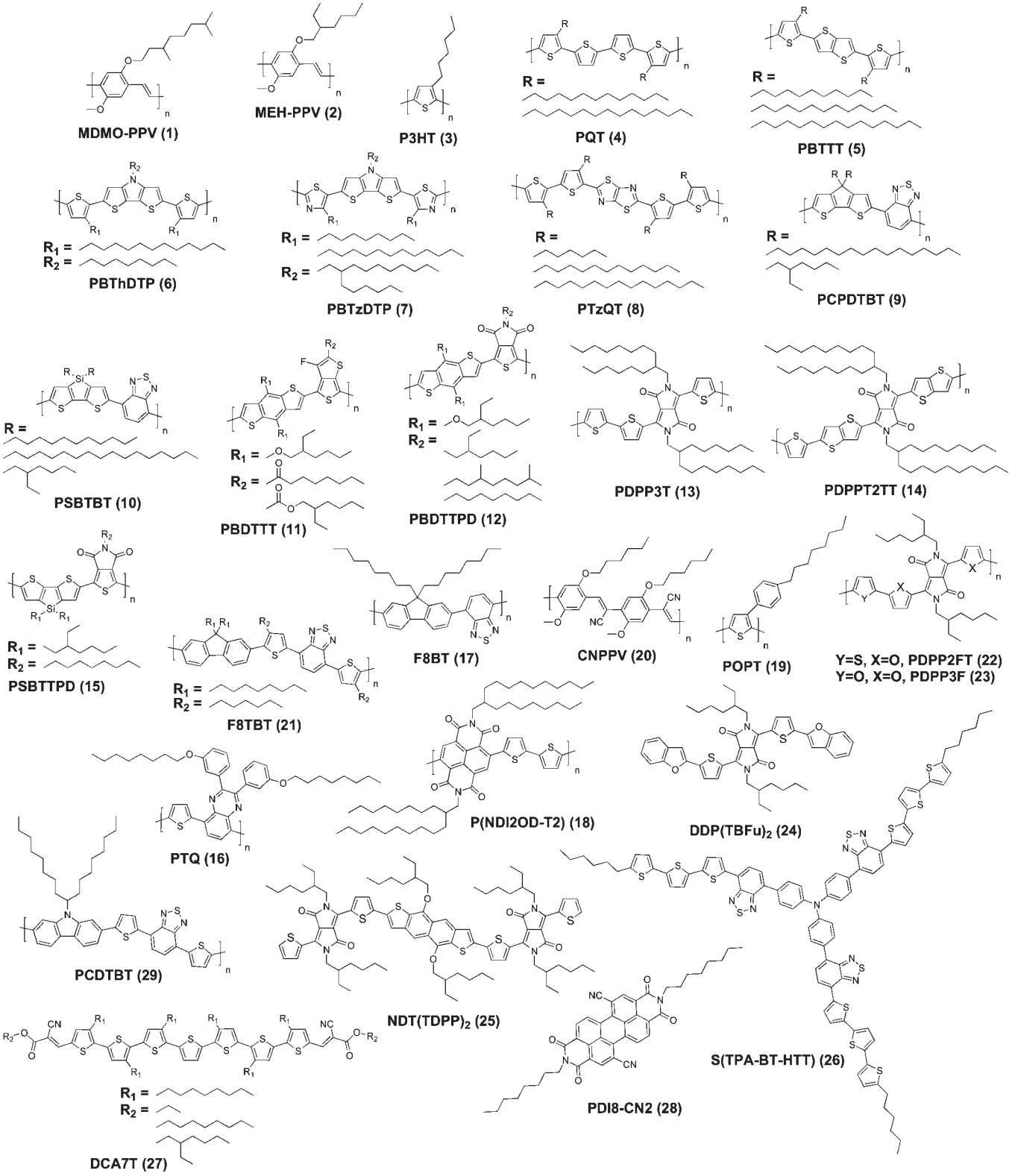

constant ($\sim 10^{-4}$ cm^2 V^{-1} s^{-1}) for (number average) MW = 13 and 18 kDa and (ii) decrease by 1 order of magnitude when MW was increased to 34−121 kDa.[18] In this instance, the variations in hole mobility with MW were found to correlate with substantial changes in thin-film morphology for blends with PCBM, leading to a subsequent drop in OPV device performance for MW > 34 kDa. Thus, it was postulated that higher MW fractions possess a higher degree of entanglement, hindering *intra*chain carrier transport by increasing the

dx.doi.org/10.1021/ja2073643 |*J. Am. Chem. Soc.* 2011, 133, 20009–20029

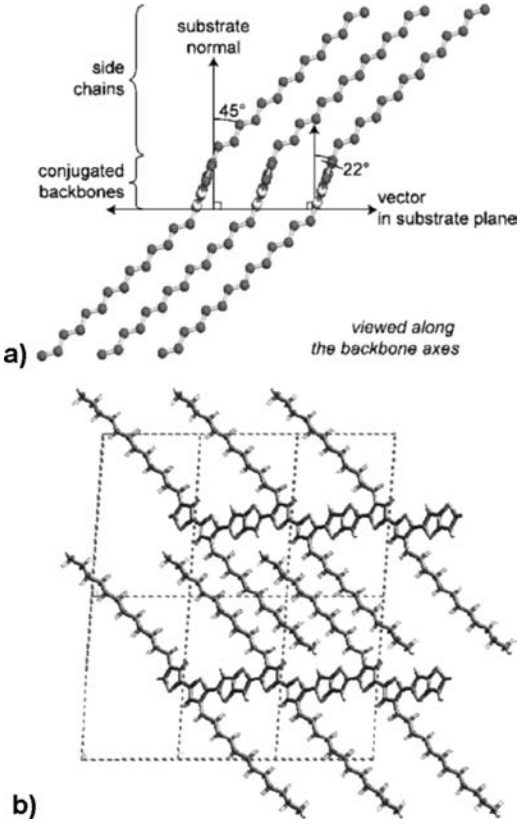

Figure 3. (a) PBTTT (**5**) backbones adopt a coplanar conformation, involving a tilt with respect to the lamella plane. Reproduced with permission from ref 24. Copyright 2007 Wiley. (b) The solubilizing side chains of PBTTTs interdigitate, thus reducing the lamellar spacing between backbones. Reproduced with permission from ref 25. Copyright 2009 Wiley.

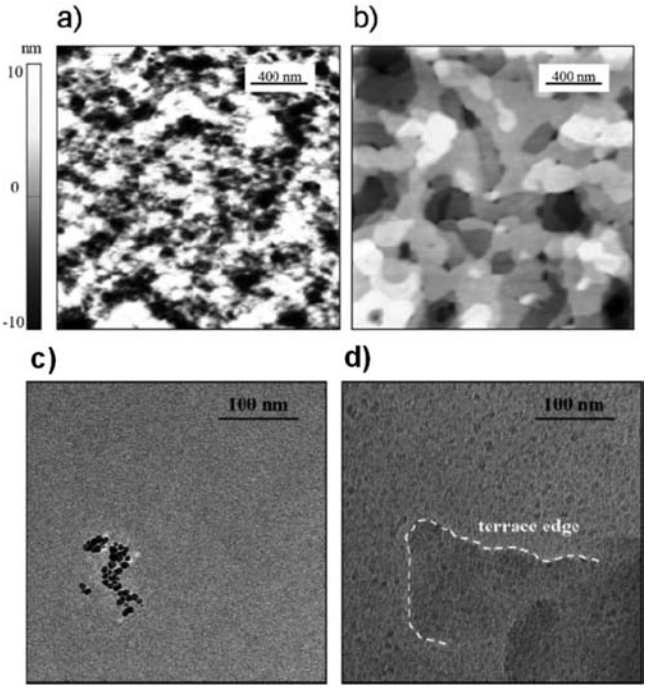

Figure 4. AFM topography images of a film of PBTTT (**5**) on OTS-treated SiO_2 (a) prior to thermal annealing and (b) after annealing into the polymer's mesophase. Large flat terraces and molecular-height steps of 250−300 nm are formed upon annealing. Bright-field transmission electron microscopy (TEM) images of PBTTT films (c) prior to thermal annealing and (d) after annealing into the polymer's mesophase (films spun on OTS-treated SiO_2 and subsequently delaminated). The TEM image in (d) reveals the existence of nanoscale features (∼10 nm in size) within the large terraces of the PBTTT film. Reproduced with permission from ref 26. Copyright 2010 Wiley.

density of traps, while also impeding *inter*chain hopping by diminishing the π-overlap between backbones. Careful investigation of the gelation mechanism, including fiber formation, of P3HT in *o*-xylene solutions has revealed a distinct two-step process involving $\pi-\pi$ aggregation and thermoreversible gelation, in a MW-dependent mechanism where individual aggregated chains link to one another.[19] OPV devices processed from *o*-xylene from various MW fractions of P3HT achieved PCEs that remained relatively constant at ∼3.6% for (weight average) MW = 43.7 and 72.8 kDa, but decreased at higher MW. One consistent trend among these studies is the observation of a clear effect of MW on the fibrillar morphology of P3HT, which affects carrier mobility and device performance.

With its particularly electron-rich π-system, P3HT also suffers from a number of limitations, including the lack of side-chain interdigitation and ordering, hindering long-range organization, and its susceptibility to ambient oxidative processes. These limitations now provide useful guidance for the synthetic design of potentially improved materials.

Poly(thieno[3,2-*b*]thiophene)s (PBTTTs, **5**, Chart 1) constitute a promising class of candidate materials in the search for high-performance organic transistors as they can crystallize with domain sizes that reach the scale of printable channel lengths (∼200 nm) and show field-effect hole mobilities reaching values (0.2−0.6 $cm^2\ V^{-1}\ s^{-1}$) comparable to those of amorphous silicon.[23] In analogy with PQTs, which have roughly similar hole mobilities (0.1 $cm^2\ V^{-1}\ s^{-1}$), the side chains of PBTTTs can interdigitate[24,25] (Figure 3), thus promoting long-range intermolecular organization. Interestingly, despite the large crystalline terraces typically observed by atomic force microscopy (AFM) (Figure 4a,b),[23,26] recent structural and morphological characterization of thin films of PBTTT suggests the existence of nanometer-scale substructures (∼10 nm in size, Figure 4c,d) similar to those seen in P3HT or PQTs.[26] Hence, the superior carrier mobility of PBTTT over that of P3HT does not necessarily stem from a reduced concentration of trap densities, which was found to be on the same order of magnitude in OTFTs made with P3HT, PQT, or PBTTT. Instead, the backbone rigidity of PBTTT, its interdigitated pattern of solubilizing side chains, and its ability to form highly regular crystallites[26] (albeit only ∼10 nm in size) is believed to be at the origin of its high field-effect hole mobility. It was shown recently that the density of abrupt grain boundaries across OTFT channels of PBTTT is relatively low and independent of processing, thus accounting for similar saturation hole mobilities and charge-carrier hopping activation energies.[27]

Semiconducting polymers that exhibit high carrier mobilities in the absence of induced macroscopic order would be ideal in the context of high-throughput manufacturing processes. Avoiding the need for tedious postdeposition solvent and thermal annealing treatments would be highly beneficial, as these steps can lead to substantial performance variations from device to device. *N*-Alkyldithienopyrrole-based polymers such as PBThDTP (**6**, Chart 1), designed to be inherently amorphous through its

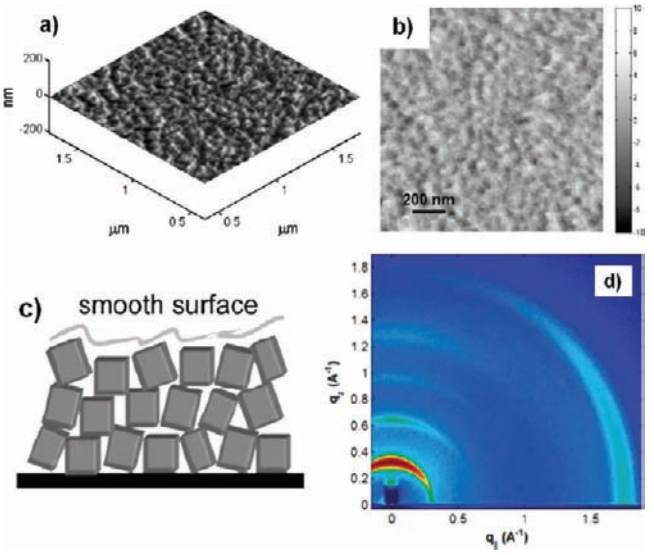

Figure 5. (a) AFM topography (3D) and (b) phase (2D) images of an as-cast thin film of PBTzDTP (**7**, dodecyl-substituted) on OTS-treated SiO_2/Si substrate. (c) Schematic representation of the postulated structural organization of PBTzDTP (dodecyl) in thin films (the blocks represent the polymer domains). The film is highly textured without extended crystalline domains. Reproduced with permission from ref 29. Copyright 2009 Wiley. (d) Grazing incidence wide-angle X-ray scattering (GIWAXS) pattern of drop-cast thin film of a thiazolothiazole−thiophene copolymer annealed at 150 °C. Lamellar (out-of-plane direction, q_z) and π-stacking reflections (in-plane direction, q_x) support the presence of nanostructural order and absence of mesoscale crystallinity (confirmed by AFM). Reproduced with permission from ref 32. Copyright 2010 American Chemical Society.

complex repeat unit and non-regioregular side-chain pattern, have recently shown "as-cast" field-effect hole mobilities of up to ~0.2 $cm^2\ V^{-1}\ s^{-1}$, albeit with low on/off ratios ($10-10^4$).[28] While the relatively high highest occupied molecular orbital (HOMO) energy states of these polymers (~4.7−5.0 eV by cyclic voltammetry) were likely responsible for the modest on/off ratios observed in OTFTs, this shortcoming has been addressed with a dithienopyrrole-based polymer analogue, PBTzDTP (**7**, Chart 1), which has electron-deficient thiazole units along its π-conjugated backbone.[29] With its slightly deeper HOMO (~5.2 eV), this polymer showed as-cast field-effect mobilities as high as 0.14 $cm^2\ V^{-1}\ s^{-1}$ and on/off ratios in the range 10^5-10^6. Devices made with this polymer showed good stability over a period of 60 days in air (~20% humidity), while AFM analyses pointed to the absence of macroscopic order (Figure 5a−c). This critical finding suggests that a high degree of thin-film crystallinity may not be required for high OTFT performance, and that relatively amorphous conjugated systems exhibiting long-range π-connectivity can challenge the performance of their semicrystalline counterparts. Similarly, thiazolothiazole−thiophene copolymers, such as PTzQT (**8**, Chart 1), with their long-range lamellar organization and pronounced propensity to π-stack (Figure 5d), have shown excellent carrier mobilities (~0.3 $cm^2\ V^{-1}\ s^{-1}$) in the absence of macroscopic order.[30−32]

While the state-of-the-art in the field of organic photovoltaics was long represented by BHJ solar cells combining P3HT and the fullerene acceptor $PC_{61}BM$, with efficiencies of ~5%, a number of π-conjugated backbones containing "push−pull" motifs—*donor−acceptor* polymers—have afforded significantly higher efficiencies. First introduced in macromolecular π-conjugated systems in the 1990s by Havinga et al.,[33,34] the donor−acceptor (DA) approach, which alternates electron-rich and electron-deficient heterocycles along the same backbone, affords polymer chromophores with narrow bandgaps, thus red-shifting their absorption spectra toward wavelengths of 500−800 nm, where the solar photon flux is most intense. The DA polymer approach has the advantages of providing both a high-lying HOMO and a low-lying lowest unoccupied molecular orbital (LUMO) within a single polymer, and minimizing the bond length alternation along the π-conjugated backbone.

Although DA polymers typically do not possess the same high degree of crystallinity in thin-film devices as their all-donor counterparts such as semicrystalline P3HT, X-ray techniques such as two-dimensional wide-angle X-ray scattering (2D-WAXS) or grazing incidence X-ray scattering (GIXRD) demonstrate that the best-performing DA polymers still show a substantial degree of microstructural order. For example,[1,35] a linearly substituted analogue of PCPDTBT (**9**, Chart 1), with hole mobility as high as 1.4 $cm^2\ V^{-1}\ s^{-1}$, exhibits a strong propensity to self-assemble in lamellar stacks. Upon further optimization, PCPDTBT reached state-of-the-art hole mobilities of 3.3 $cm^2\ V^{-1}\ s^{-1}$.[36] The same type of lamellar organization has also been observed in its branched-substituted silole analogue PSBTBT[37,38] (**10**, Chart 1), leading to solar PCEs as high as 5.6% in BHJ with $PC_{71}BM$ (**31**, see Chart 2).[39] The role of the pattern of solubilizing side chains in DA polymers (e.g., PBDTTT and PBDTTPD, **11** and **12**, Chart 1) was recently examined,[40−45] and the existence of a direct correlation between lamellar spacing and length of the solubilizing substituent was demonstrated, with several new material combinations achieving PCEs >6%.[40] Similarly, the π-stacking interaction between backbones is increasingly cited as a determining factor governing charge transport in OTFTs,[46] also impacting OPV performance. While shorter π-stacking distances tend to correlate with higher charge-carrier mobilities,[47,48] the density of π-stacked backbones within the active layer should further affect the efficiency of charge transport. In particular, the branching and bulkiness of the solubilizing side chains appended to the π-conjugated backbone may substantially affect π-stacking distances and density of π-stacked backbones.[40] In this regard, quantitative thin-film X-ray analyses[49] that subtract inaccuracies arising from thin-film inhomogeneities and beam orientation enable the comparison of diffractograms with distinct scattering intensities. This approach could ultimately help quantitate the density of π-stacked backbones, and provide a better measure of the various populations of oriented backbones across polymer thin films.

The selective introduction of fluorine atoms in the DA backbones (see PBDTTTs, **11**, Chart 1) has afforded some of the highest-performing polymers for BHJ solar cells with PCBM so far, yielding PCEs >7%.[43,50,51] In addition to lowering the HOMO and LUMO levels of the corresponding polymers, the presence of fluorine atoms along the backbones influences both π-stacking distances[51] and lamellar spacings,[50] with expected consequences on the charge-transfer complex with PCBM.[50] These studies suggest that (i) the presence of fluorine reduces polymer solubility in common organic solvents,[50] and (ii) the miscibility with PCBM tends to decrease with further additions of fluorine atoms.[51]

As was the case for P3HT, polymer MW has been reported to affect the performance of DA systems in both OTFT and OPV device architectures. These studies point to enhanced field-effect carrier mobility[35,36,52] and improved efficiencies in BHJ solar cells[53−55] with increasing MW. However, since the corresponding active layers do not possess the same degree of macroscopic

order as typically observed with the more crystalline P3HT-based thin films, it will be important to gain deeper insight into the effect of MW on the texture of active layers involving DA polymers.[52] A recent examination of the influence of polymer chain-end moieties on OPV device performance suggests that their nature does not substantially affect the optical and morphological characteristics of blends with PCBM.[56] However, significant variations in fill-factor (FF) and PCE observed upon end-group modification have been attributed to both the introduction of carrier traps and possible chemical transformations which might occur as the device is operated.

Another factor that might influence thin-film device performance is the orientation of the backbone relative to the substrate. While most solution-deposited semiconducting polymers, including P3HT,[12] PBTTT,[23] and PSBTBT,[37] tend to π-stack in a direction parallel to the substrate, the DA systems PBDTTT and PBDTTPD have been reported to possess a significant population of π-stacking planes oriented perpendicular to the substrate.[40,44] PCEs in the range of 6−8% have been demonstrated using the same DA backbones in BHJs with PCBM, representing some of the highest performance values reported to date for solution-processed organic solar cells,[40,43] and both PBDTTT[41−45,57] and PBDTTPD[40,58,59] are currently receiving a great deal of attention. Overall, it is increasingly apparent that molecular packing orientation affects not only the efficiency of charge transport but also injection and extraction of carriers in organic thin-film devices. In fact, the number of reports describing polymers combining high field-effect mobilities in lateral OTFT configurations and state-of-the-art OPV efficiencies remains very limited (e.g., PDPP3T[54] and PDPPT2TT,[60] **13** and **14**, Chart 1). For example, the study of the molecular packing of PDPPT2TT, reaching PCE = 5.4% in BHJ with $PC_{71}BM$ and up to 1.95 $cm^2\ V^{-1}\ s^{-1}$ hole mobility in top-gate/bottom-contact OTFTs,[60] will be of interest. In studying other systems, it will be essential to identify the structural and/or electronic reasons for preferential backbone orientations (e.g., molecular structure, interfacial dipoles, processing conditions, etc.). The role of substrate functionalization in directing preferential polymer backbone orientation relative to the substrate is also likely to be critical.[61]

Processing conditions are probably as critical as material design for solution-cast polymer solar cells, with material solubility impacting both material characterization and device optimization. Therefore, a number of reports have emphasized the use of solvent mixtures such as chloroform/*o*-dichlorobenzene[62] and of low vapor pressure small-molecule additives such as 1,8-octanedithiol, 1,8-diodioctane, or 1-chloronaphthalene[63−68] to process BHJs involving PCBM. Given the kinetics of polymer self-assembly, both approaches aim at promoting the formation of particularly ordered and homogeneous interpenetrating networks with nanoscale phase-separated domains matching the modest exciton diffusion length of 5−20 nm that prevails in organic electronics. Figure 6a−d illustrates the differences in nanoscale morphology for solution-processed BHJ devices involving a polymer donor particularly responsive to the presence of a small-molecule additive in the processing solvent. Solar cells cast from a solvent containing 2% 1-chloronaphthalene showed a ∼3-fold increase in PCE over those cast from the same solvent without any processing additive.[66] The cross-sectional TEMs of PSBTBT:$PC_{71}BM$ BHJs spin-cast from chlorobenzene show a coarse phase segregation between $PC_{71}BM$ (Figure 6e, darker oval-shaped regions >200 nm in diameter) and the polymer donor in the absence of processing additive, whereas the use of 1-chloronaphthalene produces a more favorable nanoscale morphology (Figure 6f).[69] Interestingly, in the latter case, the electron mobility

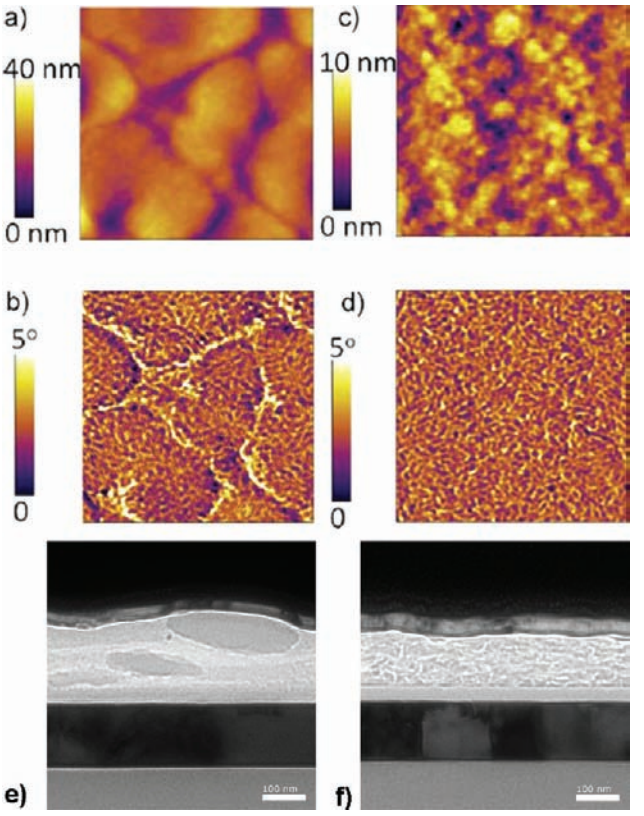

Figure 6. AFM topography (a,c) and phase (b,d) images of BHJ thin-film devices made with a blend of a narrow bandgap polymer analogue to PSBTBT (**10**) and $PC_{71}BM$ (**31**) without using the small-molecule additive 1-chloronaphthalene (a,b) and with 2% of 1-chloronaphthalene (c,d). The scan size of the images is 1 μm × 1 μm. Reproduced with permission from ref 66. Copyright 2010 Wiley. TEM cross-section images (−25 μm defocus) of PSBTBT:$PC_{71}BM$ BHJs spin-cast from chlorobenzene solution (e) in the absence and (f) in the presence of 1-chloronaphthalene. Layers are glass/ITO/PEDOT:PSS/PSBTBT:$PC_{71}BM$/aluminum/platinum, from bottom to top. Scale bars: 100 nm. Reproduced with permission from ref 69. Copyright 2010 American Chemical Society.

of the BHJ was found to be several orders of magnitude higher, thus suggesting a more continuous pathway for electron transport. The critical role of processing additives has also been emphasized in BHJ devices made with PBDTTT,[41−45,57] PBDTTPD,[40,58,59] PSBTTPD[70,71] (**15**, Chart 1), and analogues,[71,72] yielding PCEs >7% in BHJs with $PC_{71}BM$ when an additive is used in the processing solvent. Because of the large difference in vapor pressure between solvent and cosolvent or additive, it is believed that the final morphology is essentially dominated by the evaporation of the lower vapor pressure cosolvent or additive. This process allows the polymer chains to slowly crystallize, and continue arranging after the higher vapor pressure solvent is evaporated. Similarly, processing additives able to solubilize PCBM (Figure 7) may prevent its rapid crystallization and, in turn, the formation of large segregated domains.[65] In general, it may be stated that the most (semi)crystalline systems will be more responsive to postdeposition thermal annealing treatments, while the more amorphous ones will often benefit from the use of low vapor pressure solvents and additives. Morphological models may allow predicting device performance improvements achievable by

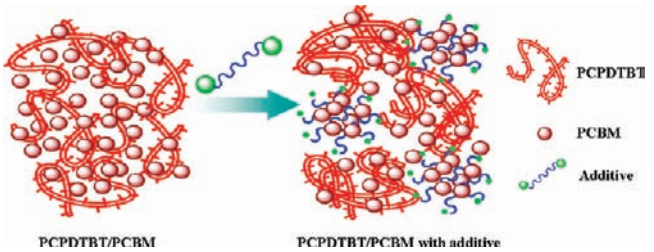

Figure 7. Schematic representation of the role of the processing additive in the self-assembly of the BHJ blend components. Reproduced with permission from ref 65. Copyright 2008 American Chemical Society.

further optimizing blend morphologies until the most favorable configuration can be obtained.[73]

Despite their near-identical molecular structures, PCPDTBT and PSBTBT exhibit subtle differences in thin-film ordering properties, yielding distinct performance profiles in both OTFTs and OPVs.[37,38] In particular, the nature of the bridging atom (C or Si) is believed to impact the substitution pattern of solubilizing side chains by governing the bond angles at the neopentyl center and, in turn, the molecular packing. As a result, favorable nanoscale morphologies on the order of the exciton diffusion length are best formed with PCPDTBT:PCBM blends containing small-molecule additives,[68] while favorable morphologies with particularly crystalline PCBM domains are reached with additive-free PSBTBT:PCBM blends.[74] Importantly, favorable nanoscale phase separations achieved with these systems were shown to "deactivate" the charge-transfer complexes typically involved in multistep recombination processes at the DA interface, which correlated with enhanced overall device efficiency.[74]

In the context of BHJ optimization, the determination of the ideal polymer:PCBM blend ratio has been a matter of trial and error so far, with 1:1 and 1:3−4 ratios used most frequently. A recent report exploring BHJs of PBTTT with PCBMs of various sizes suggests that fullerenes can intercalate between the side chains of π-conjugated polymers (Figure 8).[75] In this study, blends in which $PC_{71}BM$ was found to intercalate along the PBTTT backbone showed optimized solar cell performance upon incorporation of 4 equiv of the fullerene, whereas only 1 equiv of the substantially larger $BisPC_{71}BM$ derivative (**32**, see Chart 2) was needed to reach an optimized device configuration. This empirical observation is consistent with the notion that a polymeric system allowing PCBM to intercalate may require a larger number of equivalents of fullerene to achieve a favorable nanoscale phase separation. Following these considerations, a rapid overview of the π-conjugated polymers possessing a lower density of solubilizing side chains along their backbones indicates that a greater number of PCBM equivalents are indeed generally employed to produce devices performing under optimized conditions.[76−78] Importantly, the intimate mixing of PCBM with polymer donors, such as MDMO-PPV,[79] is known to improve the hole mobility of the blends by up to several orders of magnitude compared to the pristine polymer.[80] These empirical results support the idea that the presence of PCBM can improve the molecular packing of the polymer in blends, and ultimately device operation. At the same time, it is worth noting that when larger PCBM loadings are incorporated, the optical density of the resulting active layer decreases at long wavelengths where the solar photon flux is the most intense, and this alone may

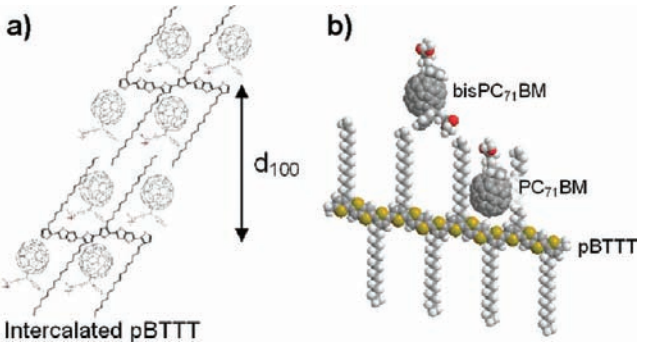

Figure 8. (a) Schematic representation of a network of PBTTT (**5**) backbones intercalated with $PC_{71}BM$ (**31**). (b) The second solubilizing substituent of $BisPC_{71}BM$ may prevent the intercalation of this larger fullerene in the free spaces between the side chains of PBTTT. Reproduced with permission from ref 75. Copyright 2009 American Chemical Society.

ultimately constitute the most limiting factor with respect to device performance. Interestingly, despite their excellent field-effect carrier mobilities, or the long-range order achievable in thin films, semicrystalline PBTTTs have reached only limited PCEs in BHJs with PCBM (~2.3% with $PC_{61}BM$).[81] Considering the mismatch between electron and hole mobilities (dominated by space charge regimes) in the direction normal to the substrate, the usable device thickness is limited to ~115 nm, thus limiting the capture of incident radiation and the photogenerated current.

A recent report suggests that interdiffused active layers obtained by sequential solution deposition and diffusion of a top layer of PCBM cast on a bottom layer of polymer donor—"layer-evolved BHJs"—can show improved vertical connectivity compared to conventional BHJs.[82] Sequential solution-processing approaches could prove useful in controlling the formation of BHJ nanoscale morphologies. In parallel, it is worth noting that interdiffusion of PCBM can also be induced in a bilayer device subjected to thermal annealing.[83]

Maximum efficiency for organic solar cells has so far been achieved with films 90−120 nm thick, and efficiency is usually lowered with significantly thicker films as a result of the low dielectric constant and high recombination rates that prevail in organic electronics. Reduced current densities and lower FFs are the hallmarks of charge-transport limitations across these active layers. Film thickness limitations raise a number of challenges as we aim to implement solution-processable organics in devices via roll-to-roll film-deposition processes for which ~200 nm thick films are typically deposited.[84] It is important to note that increasing active-layer thickness could contribute to substantially larger external quantum efficiencies (EQE_{PV}) to afford PCEs exceeding 10%. The case of P3HT, for which peak solar cell performance has frequently been achieved with active layers exceeding 150 nm, has long remained relatively unique.[85] Interestingly, PTQ (**16**, Chart 1), which combines FFs approaching 70% with open-circuit voltage (V_{OC}) of ~0.9 V, and yields PCEs of ~6% in BHJs with $PC_{71}BM$, was recently found to maintain high short-circuit current (J_{SC}) values and excellent FFs for active-layer thicknesses in excess of 200 nm.[86] Similarly, PSBTTPD maintained ~6% PCE for active-layer thicknesses of 220 nm.[70] It will be of interest to identify the material properties—degree of thin-film structural order in particular—imparting this

specificity to PTQ, PSBTTPD, and other similarly promising DA systems.[51,84]

The stability of polymer solar cells is a matter of increasing interest. To bring OPVs one step closer to viable commercial applications, the parameters influencing device lifetime should be more clearly identified, and cost-effective solutions will have to be implemented. While a number of practical approaches such as module encapsulation and the use of UV-blocking front sheets are envisioned to protect the active layer from photo-oxidative degradation processes and moisture uptake, morphological stability issues are much less discussed, yet they are probably equally important. Over time,[87] and upon prolonged exposure at elevated temperatures,[88,89] discrete crystallization of the donor and acceptor components within BHJs leads to slow phase demixing events, which can seriously compromise device performance. Considering the level of molecular and thin-film engineering sometimes required to induce the most favorable nanoscale morphology, strategies are being developed to ensure that the optimized morphology is retained over time, under prolonged radiation exposure, or when subjected to thermal events. For example, the UV photo-cross-linking of a P3HT derivative possessing bromine-terminated alkyl side chains has been employed to "freeze" morphology and induce thermal stability over time, with little effect on structural properties such as π-stacking or device performance.[88] The use of solution-processing methods to prepare heterojunctions and devices with multiple layers requires that repeated depositions be carried out from orthogonal solvent systems, each of which must not disrupt the previously coated layer of organic material. Since most organic electronic materials are soluble in the same solvent systems, this constraint narrows the scope of material combinations that can be integrated in the same active layer. Here, π-conjugated polymers containing cross-linkable functionalities,[88,90] as well as cross-linkable additives blended within the active layer at the solution-deposition stage,[91] provide access to material combinations with long-term stability. Taking advantage of the ability to freeze a given morphology, cross-linked continuous networks of polymer donor and columnar assemblies produced using a sacrificial phase-directing agent (PDA) have been successfully back-filled with various electron-acceptor materials (e.g., PCBM and F8BT, **17**, Chart 1) to yield heterostructures with performance characteristics approaching or exceeding those obtained in optimized conventional devices processed from material blends.[91] Figure 9 illustrates how the sacrificial PDA can be used to produce columnar and poriferous nanostructures, as confirmed by AFM. As the mismatch between phase separation length scale in the DA network and exciton diffusion length gets reduced, it is expected that charge dissociation efficiencies will improve and that the recombination densities will be minimized. In this context, electron-accepting materials commonly avoided for their strong propensity to phase-segregate from polymeric donor materials could ultimately be employed. It is worth noting that several approaches to immobilize organic active layers relying on cross-linkable side chains and end groups have also been reported in the related area of OLEDs.[92−96]

To date, the concept of an "all-polymer solar cell" remains a largely unsolved challenge, as little headway has been made since the 1990s.[97,98] In this area, a number of parameters, including morphology, exciton diffusion length, and efficiency of charge dissociation, have commonly been held responsible for the low device efficiencies. With a wide range of new polymeric semiconductors now accessible, including higher carrier mobility DA

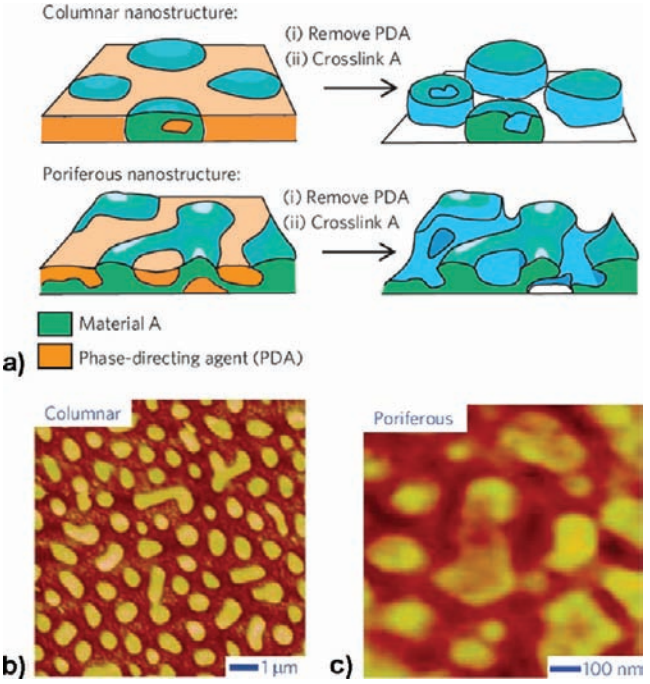

Figure 9. (a) Schematic representation of the phase separation mediated by a phase-directing agent (PDA), yielding (b) columnar or (c) poriferous (sponge-like) nanostructures. Spontaneous demixing is followed by removal of the PDA and photo-cross-linking of the nanostructured component A, over which component B can be deposited to produce the interpenetrating heterostructures. AFM images, image height = 30 nm. Reproduced with permission from ref 91. Copyright 2010 Nature Publishing Group.

π-conjugated systems, the all-polymer device configuration may be expected to receive more attention in the near future. However, as suggested by the very low PCE values of only 0.2% achieved with BHJs of P3HT donor and P(NDI2OD-T2) (**18**, Chart 1) acceptor,[99] the combination of high carrier mobilities and suitable energy level offsets will not be sufficient to overcome the charge separation issues in systems dominated by geminate recombinations. Among other requirements, achieving a favorable nanoscale morphology is a must! It is therefore critically important to develop novel strategies to achieve morphology control independent of the materials processed, while continuing to acquire a deeper understanding of charge separation dynamics.[100,101]

An excellent illustration of how simple changes in molecular structure impact the efficiency of all-polymer systems is provided by a comparative study of the donor polymers P3HT and poly[3-(4-*n*-octyl)-phenylthiophene] (POPT, **19**, Chart 1) in bilayer laminate devices with the electron acceptor CNPPV (**20**, Chart 1). While non-regioregular POPT had initially demonstrated particularly high photocurrents and EQEs in comparison with P3HT (yet with PCE < 0.5%),[102] regioregular POPT has since afforded up to 2% PCE with CNPPV (vs <1% with regioregular P3HT),[103] a result which constitutes the highest performing all-polymer solar cell device to date. Given the comparable spectral absorption and hole mobility of the two regioregular analogues, the charge photogeneration enhancement seen with POPT/CNPPV may be attributed to a destabilization of the ground-state charge-transfer intermediate (i.e., geminate electron−hole pair) caused by a twist of the sterically demanding 3-phenyloctyl pendant group, which controls the intermolecular

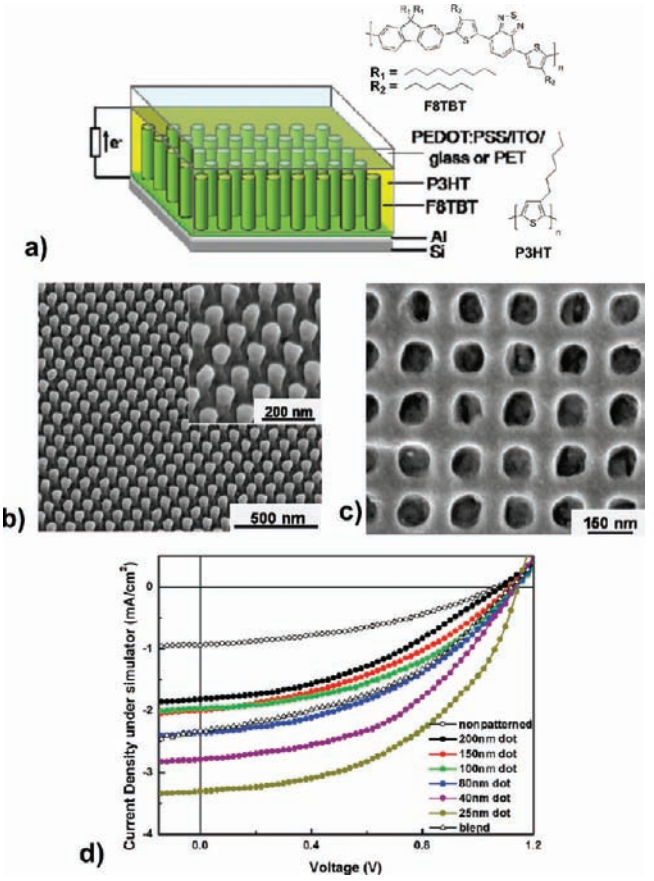

Figure 10. (a) Schematic representation of a nanoimprinted heterojunction solar cell device of P3HT (**3**) and F8TBT (**21**). A patterned film of P3HT is used as a mold to imprint a film of F8TBT spin-cast on an Al-coated Si wafer. Scanning electron microscopy (SEM) images of (b) ~80 nm posts imprinted in the P3HT films via a Si master and (c) the ~80 nm holes subsequently imprinted in F8TBT by the patterned P3HT film. (d) $J-V$ characteristics for double-imprinted devices with various interdigitated feature sizes, and for planar and blend controls, under solar illumination conditions. Reproduced with permission from ref 104. Copyright 2009 American Chemical Society.

distance between polymer donor and neighboring acceptor molecule. The destabilization of this intermediate would indeed be expected to facilitate the generation of free charges, thus inducing higher photocurrents. This design principle should be applicable to other systems including DA polymers, and the combination of structurally modified polymer donors such as POPT with new, higher-performing polymer acceptors should contribute to improve the efficiency of all-polymer bilayer devices.

Work on interdigitated heterojunction all-polymer solar cells provides compelling evidence that control over phase intermixing and domain size represents the most critical challenge. Thus, controlled interpenetrating columnar morphologies with varying densities of interdigitated features (up to 10^{14} mm^{-2}) were produced by successive nanoimprinting steps to demonstrate how domain size and DA surface area affect solar cell efficiency in heterojunction devices of P3HT and F8TBT (**21**, Chart 1, and Figure 10).[104] Interdigitated junctions with feature sizes on the order of the exciton diffusion length of this system (≤25 nm) produced PCE values as high as 1.9%, FF ≈ 50%, V_{OC} = 1.14 V, and EQE_{PV} values peaking at 26%, which are among the highest

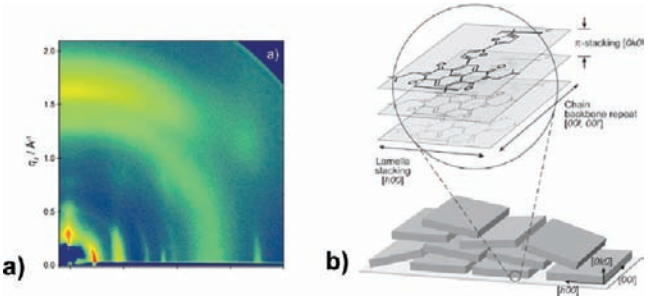

Figure 11. (a) 2D grazing incidence X-ray scattering pattern of a spin-cast film of P(NDI2OD-T2) (**18**), suggesting pronounced in-plane ordering, yet limited out-of-plane π-stacking propensity. (b) Schematic representation of the preferential face-on backbone orientation shown by P(NDI2OD-T2), and the plausible microstructural organization in thin films. Reproduced with permission from ref 110. Copyright 2009 Wiley.

reported values to date for all-polymer solar cells. In comparison, the BHJ of P3HT and F8TBT yielded only 1.1% PCE, while a "control" bilayer device showed <0.4% PCE. Of course, the same approach can be applied to heterojunctions of polymer donors and PCBM[105] to study various material combinations using the same nanoscale morphology.

High-mobility electron-transporting polymers remain an elusive class of materials. While polymers that can be used as the electron-accepting component in BHJ solar cells are sparse (e.g., CNPPV,[97,98,102] F8BT,[106] and F8TBT[104,107]), only a limited number—potentially useful for efficient n-channel OTFTs—are solution-processable and relatively stable to ambient oxidative processes. Among these, P(NDI2OD-T2)[108] shows electron mobilities as high as 0.85 cm^2 V^{-1} s^{-1}, relatively low turn-on voltages of <5 V in top-gate device configuration, and excellent ambient stability over several weeks of operation.[109] Inspection of the molecular packing and thin-film microstructure of P(NDI2OD-T2) by GIXS revealed pronounced in-plane ordering with limited out-of-plane π-stacking propensity, and suggested a predominant "face-on" backbone orientation relative to the substrate (Figure 11).[110] In such an orientation, it is possible that charge carriers can bypass trap states at the dielectric interface by hopping to the most directly accessible layers along the out-of-plane π-stacking direction. Similarly, DA systems with preferential "face-on" orientation in thin films and hole mobilities of ~1 cm^2 V^{-1} s^{-1} have recently been reported.[111] Remarkably, backbone reorientation can be induced by melt-anneal processes in thin films of P(NDI2OD-T2), leading to "edge-on" textures with improved crystallinity.[112] Further examination and control over the backbone orientation at the substrate interface may allow improving in-plane mobilities in bottom-gate OTFTs made with P(NDI2OD-T2). The implementation of novel synthetic approaches to producing polymers solely composed of electron-deficient building units should prove useful in the development of efficient n-type materials for both OPV and OTFT applications.[113]

A number of recent studies have focused on the fundamental properties and potential of selenophene-derivatized polymer semiconductors in both OTFTs and OPVs. For example, poly(3-hexylselenophene) (P3HS) possesses a lower bandgap (1.6 eV) than P3HT (1.9 eV); hence, it is able to harvest more light and produce larger photogenerated currents in solar cells while maintaining a similar ionization potential (4.8 eV).[114] Early characterization of P3HS in p-channel OTFTs[114] and BHJs

with PCBM[115] suggests that the selenophene analogue could ultimately outperform P3HT, provided that a microstructural organization favoring lower charge recombination densities in BHJs can be obtained.[116] Detailed studies of the charge dynamics governing polyselenophene-based thin-film devices will provide further insight into the structural barriers that must be overcome, including material design, device geometry, and morphology.[116,117] The π-system of P3HS is characterized by significant localization of the HOMO on the carbon backbone rather than on the heteroatoms. As a result, the influence of the larger and more polarizable selenium atom on hole transport remains low. In contrast, it will be of interest to see how the presence of selenium localizing the LUMO to some extent in P3HS[114] affects the electron mobilities in narrow-bandgap DA semiconducting polymers. In fact, the ambipolar charge-transport character of polyselenophenes was emphasized in a recent report where matched electron and hole mobilities of ~0.03 $cm^2\ V^{-1}\ s^{-1}$ were achieved.[118] It is expected that the development of new building block will lead to further improvements.[119] Initial characterization of the thin-film morphology of poly(3-hexylselenophene-*block*-3-hexylthiophene)s shows that nanoscale phase separation occurs between the thiophene- and selenophene-rich blocks—a result that supports the existence of substantial physical/electronic property differences between the two analogues.[120]

Surprisingly perhaps, furan-containing polymeric systems have attracted very little attention. While only a few furan-containing polymers had been explored for electronic device application,[121] the low-bandgap polymer PDPP2FT and its all-furan PDPP3F counterpart (**22** and **23**, Chart 1) have recently been reported to afford average PCEs of 4.7% and 3.8%, respectively, in BHJs with $PC_{71}BM$.[122] Such efficiencies are comparable to those produced earlier with the all-thiophene analogue PDPP3T (4.7%).[54] A clear benefit resulting from the incorporation of furan along the polymer backbone is higher solubility, enabling the use of solubilizing groups shorter than those required for the all-thiophene analogue PDPP3T. This design principle[95] could be applied to a variety of other systems for use in OPVs and OTFTs, with the ultimate aim of enhancing processing properties as well as device performance. Early work with furan-containing polymers shows that promising hole mobilities can be achieved in OTFTs.[123]

SOLUTION-PROCESSED SMALL MOLECULES

While vapor deposition or patterning methods and relatively high temperature annealing steps have long been thought to be requirements for small-molecule OTFT performance, simple methodologies inducing ideal morphologies, which can be accessed under rapid solution-processing conditions, are now emerging. A convenient approach to inducing microstructural order without using any specific alignment processing technique involves engineering the contact interface before deposition, as demonstrated in solution-cast acene-based OTFTs.[124] Following this strategy, the selective growth of highly textured organic thin films can be extended from the chemically modified contact electrodes into the transistor channel to yield field-effect mobilities several orders of magnitude larger than those obtained with conventional spin-coated active layers. As solvent vapor annealing approaches are proving increasingly relevant, more fundamental understanding of the molecular ordering process taking place upon solvent evaporation should be developed. While the combination of time-resolved optical reflectometry and time-resolved grazing incidence X-ray techniques has already proven useful in the characterization of solvent-annealed crystallites of "insoluble" pentacene,[125] the same technique could also be used to provide more precise mechanistic understanding of the successive intermolecular ordering events that take place during the solution deposition of organic semiconductors. Alternative solution-processing techniques include inkjet printing,[126] although forming highly ordered thin-film patterns by the conventional printing approaches has commonly been described as a challenge to be addressed in order to maximize OTFT mobilities. In this area, antisolvent crystallization techniques[127] introduce a promising platform for the implementation of highly crystalline active layers of solution-processed small molecules.

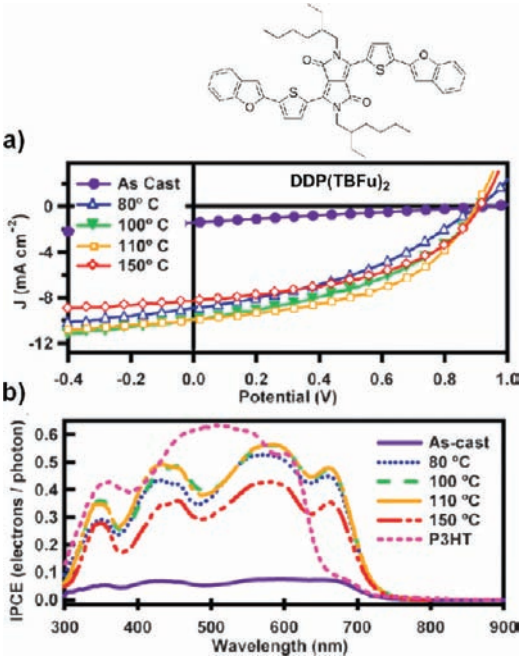

Figure 12. (a) $J-V$ characteristics and (b) external quantum efficiencies (EQE_{PV}) of BHJ solar cell devices combining $DPP(TBFu)_2$ (**24**) and $PC_{71}BM$ (**31**) (60:40), and annealed at different temperatures. The EQE_{PV} of an optimized P3HT:$PC_{61}BM$ device is superimposed for comparison. Reproduced with permission from ref 131. Copyright 2009 Wiley.

π-Functional small molecules benefit from the fact they are easy to purify, tend to possess high intrinsic carrier mobilities, and are able to self-assemble to achieve long-range order. While an impressive library of oligomers of thiophenes has been built and explored over the past two decades,[128−130] symmetrically designed DA small molecules appended with solubilizing substituents, and consisting of an electron-deficient core flanked with electron-rich units, are now being considered as alternatives to their all-donor counterparts. Specific applications for these narrow-bandgap derivatives include photovoltaics, for which light absorption is a critical parameter, n-channel or ambipolar transistors using low-lying LUMO energy states to transport electrons, and even more complex device configurations such as complementary inverters. Beyond electronic and spectral considerations, the lack of control over the morphologies produced with crystalline oligomers of thiophene—often dominated by the rapid formation of overly grown crystallites—is frequently cited as the cause for both pronounced phase separation in BHJs and interfacial delamination in OTFTs. An illustration of the recent progress made in the area

of solution-processed small-molecule OPVs involves a diketopyrrolopyrrole (DPP)-based DA molecule containing both thiophene and fused benzofuran building blocks, namely DPP(TBFu)$_2$ (**24**, Chart 1), which demonstrates up to 4.4% PCE and FF = 48% in BHJ with PC$_{71}$BM (Figure 12).[131] These excellent early results have been attributed to a variety of contributing parameters, including (i) high optical density in the range 500−700 nm; (ii) a relatively large electron affinity improving the match between small-molecule LUMO and that of PCBM while maintaining a driving force of ∼0.3 eV for charge transfer; (iii) the central position of the solubilizing side chains; (iv) the presence of benzofuran moieties stabilizing the HOMO of the system to maximize device V_{OC} (∼0.92 eV); and (v) the favorable film-forming properties in blends with PCBM.[131] Further examination of BHJ solar cells based on DPP(TBFu)$_2$ and PC$_{61}$BM revealed that charge recombination rates in the blend are especially high under 1 sun illumination (100 mW cm^{-2}), which limits the FF. In contrast, a peak PCE = 5.2% was reached by reducing the density of photoinduced carriers under a weaker irradiation intensity of 11 mW cm^{-2}, at which the FF was higher.[132] In the case of NDT(TDPP)$_2$ (**25**, Chart 1), the combination of a broad spectrum and high absorption coefficients in the 500−700 nm range leads to EQE$_{PV}$ values reaching 68%.[133] These findings support the use of relatively large yet well-defined discrete molecular entities as alternatives to polymers. If charge recombination processes can be overcome, it is clear that DPP-based[131,133−138] and other small molecules[139−142] could soon challenge polymeric systems as solar cell materials.

Because the charge transport in small-molecule-based BHJs is dominated by hopping, the degree of π-electronic overlap between molecules in the presence of PCBM is expected to exert a great influence on device FF. However, shunt and series resistance in OPVs remain largely influenced by morphological parameters, including the presence of structural inhomogeneities, interfacial disconnects, and the density of grains in highly crystalline active layers. Overall, the device FFs of 30−50% typically estimated in small-molecule BHJs[131,143−147] tend to be substantially lower than those observed in their polymer-based BHJ counterparts where they reach values of 50−70%.[39,40,43,62] Therefore, it will be important to continue exploring ways in which small-molecule-based device FFs can be enhanced in order to achieve PCEs that match those presently achieved with π-conjugated DA polymers.

The case of a low-energy small-molecule absorber used to sensitize a BHJ made with P3HT and PCBM, and yielding higher photocurrents and a somewhat larger V_{OC} than the control device without the small molecule, is worth mentioning.[134] This approach, building on a given complementarity, for example spectral or morphological, between π-functional small molecules and polymers, suggests an interesting new route to optimize device performance.

Solution-processable squaraine[148] dyes have recently been used as the electron-donor component in BHJs with PCBM.[149−151] Interestingly, in these systems, even minimal molecular structure variations induced at the termini of the solubilizing side chains (*n*-hexenyl vs *n*-hexyl) were shown to produce significant changes in OTFT and OPV performance.[150] Thus, the use of *N*-alkenyl side chains afforded more compact solid-state packing configurations, yielding a 5-fold increase in field-effect mobility and a 2-fold improvement in solar cell efficiency, reaching PCE ≈ 2%. For a different dye, OPV device efficiency was found to be greatly dependent on the ratio of squaraine to PCBM employed as it affects both the nanoscale morphology and the hole mobility of the blend.[151] At optimized blend composition, PCE = 2.7% was reached. These results further emphasize the critical need to maintain effective feedback loops between synthetic design and device characterization/optimization in general.

Star-shaped π-functional small molecules are another very promising class of solution-processable systems for BHJ solar cell device applications.[143,152] In particular, PCEs in excess of 4% in BHJs with PC$_{71}$BM have recently been obtained with DA analogues, such as S(TPA-BT-HTT) (**26**, Chart 1), which absorb more effectively in the long-wavelength region of the visible spectrum.[153] The values V_{OC} = 0.87 eV and FF = 52% achieved with this system largely contribute to the high PCE values. Notably, these results were obtained in the absence of small-molecule processing additives, and without resorting to a postprocessing treatment such as thermal or solvent-vapor annealing.

Oligomers of thiophenes end-functionalized with alkyl cyanoacetate electron-withdrawing substituents, namely DCA7T (**27**, Chart 1), achieve "as-cast" PCEs over 5% in BHJ with PC$_{61}$BM.[154] Here again, the large V_{OC} = 0.86 eV and FF = 55% greatly contribute to device PCE. This finding provides another example of a favorable nanoscale morphology achieved in the absence of postprocessing treatment of the active layer. Interestingly, in this case, changing the nature of the alky end-substituents did not induce major variations in device performance with PCEs remaining >4%.

As higher-performing n-type semiconducting small molecules[155−166] are developed for OTFTs, it is important to understand how microstructural order correlates with electron transport in highly crystalline lattices. When large crystalline monodomains with different orientations are formed within the thin-film active layer, grain boundaries are introduced, which can dominate carrier transport. This is exemplified in thin films of the perylenediimide PDI8-CN$_2$ (**28**, Chart 1), where field-effect electron mobilities have recently been shown to differ by ∼2 orders of magnitude as a function of grain-boundary orientation.[167]

Overall, in order to fully exploit the intrinsic performance capabilities of small-molecule semiconductors, it appears that a relatively high degree of microstructural order extending over large crystalline domains may have to be induced. At the same time, strategies aimed at improving the interconnection between crystallites could also greatly improve charge-carrier transport in these systems. In most studies, microstructural organization is promoted in a postdeposition annealing step, and small molecules for which optimal device characteristics can be obtained "as-cast" remain rare.

■ ARE THERE ALTERNATIVES TO PCBM?

The bulk of studies on organic photovoltaics has involved PC$_{61}$BM and its longer-wavelength-absorbing analogue PC$_{71}$BM, yet it is possible that alternative structures could outperform these two benchmark compounds.[168−172] Thus, in recent work, an indene-C$_{60}$ bisadduct (ICBA, **33**, Chart 2), has outperformed PC$_{61}$BM in BHJ with P3HT,[169,173] affording high photocurrents and V_{OC} ≈ 0.84 V with PCEs as high as 6.5%. Such findings suggest that higher-lying LUMO (i.e., lower electron affinity) fullerenes could be used in BHJ with deeper-lying HOMO (i.e., higher ionization potential) polymers and small molecules, including DA systems, in order to reach V_{OC} values approaching or even exceeding 1 V.

Chart 2

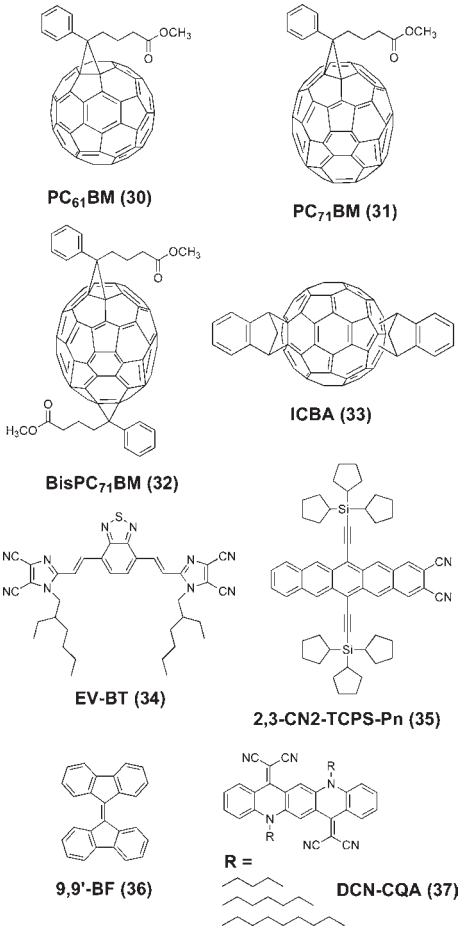

The use of a substituted fullerene derivative that yields C_{60} upon *in situ* thermolysis is worthwhile noting.[174] While C_{60} itself is prone to aggregation and difficult to process in BHJ devices with polymer donors, the ability to produce the bare fullerene via a postdeposition thermal annealing step may yet lead benefits as it is likely to influence molecular packing and blend morphology.

To date, few promising alternatives to spherical fullerenes have been uncovered. While perylenediimides (PDIs) have been extensively explored with a variety of electron donors such as P3HT[175,176] and polycarbazoles,[177] they have met with limited success,[178] affording PCEs <1% under 1 sun despite their high electron mobilities and substantial exciton diffusion lengths. Electron trapping by small crystalline domains of PDI has been suggested as a barrier for achieving large photocurrent densities with this system, although this problem may be partly circumvented by careful control of the crystal lattice formation.[175] Interestingly, Vinazene-based small-molecule acceptors[179−185] such as EV-BT (**34**, Chart 2) have shown some promise in both bilayer and BHJ solar cell configurations. For example, PCEs reaching 1% in bilayer configuration and 1.4% in BHJ with POPT have recently been reported.[181] While soluble pentacenes such as TIPS-pentacene have traditionally been used as p-type components in OTFTs and OPVs, derivatives functionalized with electron-withdrawing substituents such as 2,3-CN2-TCPS-Pn (**35**, Chart 2) have recently been explored as fullerene replacements in BHJs with P3HT.[186−188] Based on theoretical insights into the pentacene:PCBM heterojunction,[189] the efficiency of charge dissociation and the density of recombinations at the interface between polymer donors and 2,3-CN2-TCPS-Pn acceptor analogues could be influenced by (i) the relative molecular orientation between the pentacene acceptor and the electron-donor component, and (ii) the degree of electronic coupling between molecular exciton and charge-transfer, or charge-separated, states. Ultimately, the modeling tool could help identify precise design principles for the synthesis of small-molecule alternatives to fullerenes.

Polycyclic structures based on electron-accepting 9,9′-bifluorenylidene cores (9,9′-BF, **36**, Chart 2) have also been described as synthetically accessible and tunable potential alternatives to PCBM.[190,191] While these systems are forced into planarity in their ground state, the addition of one electron relieves the steric strain caused by the presence of the C9−C9′ double bond, and induces the formation of a fluorenide anion with added aromatic character. Initial characterization of BHJs with P3HT has revealed a particularly high V_{OC} = 1.1 eV—nearly double that produced with PCBM—and a respectable FF = 40%, yielding PCEs as high as 2%.[190]

DCN-CQAs (**37**, Chart 2) have recently been reported as a promising class of small-molecule electron acceptors, achieving 1.6% PCE and 57% FF with P3HT as the polymer donor.[192] The spectral absorption of DCN-CQAs shifted in the 550−700 nm region complements nicely that of the relatively wide bandgap polymer P3HT, and may provide for higher photoconversion efficiencies in this key region of the spectrum. Notably, the BHJ nanoscale morphologies were largely influenced by the nature of the solubilizing side chains appended to the acceptor, which impacted device PCE. Further synthetic modifications of the substitution pattern in DCN-CQA derivatives, and careful control of the blend morphologies with polymer donors may improve these early results.

The design and synthesis of n-type semiconducting polymeric alternatives to PCBM represents another major challenge in the field of organic electronics. Though a number of n-type semiconducting polymers have been explored as electron-acceptor components in all-polymer solar cells, CNPPV remains one of the best candidates to date,[97,102] though it only affords efficiencies of up to 2%.[103] Such modest performance likely results from issues of (i) unfavorable nanoscale morphologies, (ii) charge separation, and (iii) charge transport to the electrodes. The low electron mobilities typically found in polymeric systems are also likely a contributing factor at the origin of modest performance. In addition, the lack of polarizability of the π-conjugated backbones as well as their low dimensionality when compared to spherical fullerenes, may substantially hinder their propensity to dissociate and transport charges across the polymer blends. At present, all-polymer solar cells lag behind polymer/PCBM heterojunctions in terms of performance, and alternative polymer blends promoting electron mobility and exciton dynamics—including diffusion and dissociation—remain to be found.[113]

Inorganic nanoparticles such as quantum dots, nanorods, and branched nanostructures such as tetrapods constitute an interesting alternative to fullerenes in BHJ solar cells. Polymer donors including P3HT,[193−199] MEH-PPV,[200] other phenylene-based systems,[201−203] and more recently the narrow-bandgap PCPDTBT[204] have been blended with inorganic nanoparticles to afford solar cell efficiencies as high as 3.1% (Figure 13). The case of PCPDTBT blended with CdSe tetrapods is especially significant considering the breadth of its EQE_{PV} spectrum, exceeding 30% in the range 350−800 nm and peaking at 55% in the

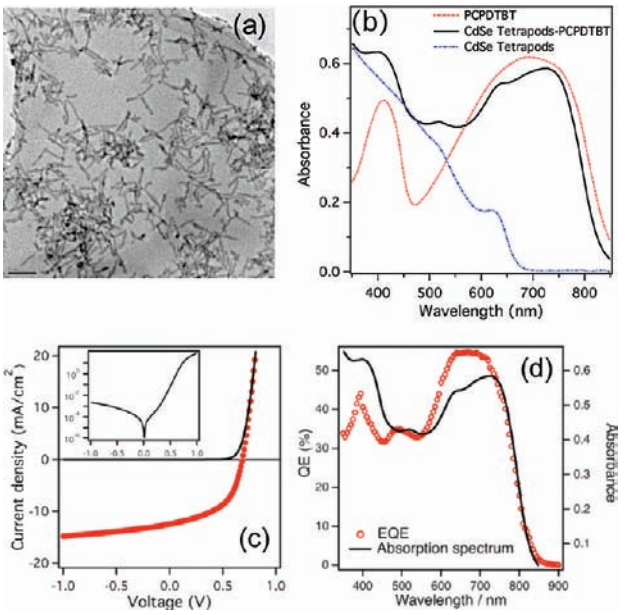

Figure 13. (a) TEM of CdSe tetrapods (scale bar: 50 nm), (b) Absorption spectra of films of CdSe tetrapods (dot-dashed, blue), PCPDTBT (**9**) (dotted, red), and their blend (solid, black), (c) $J-V$ characteristics and (d) EQE_{PV} of a BHJ solar cell device combining the narrow bandgap polymer PCPDTBT and CdSe tetrapods (under AM 1.5 global); inset shows the dark current. The absorption spectrum of the blend is shown for comparison. The PCPDTBT:CdSe hybrid device shows J_{SC} = 10.1 mA/cm^2, V_{OC} = 0.678 V, FF = 51%, and PCE = 3.19%. Reproduced with permission from ref 204. Copyright 2009 American Chemical Society.

range 630−720 nm. Organic−inorganic hybrid semiconducting blends have significant potential as they provide both solution-processability and the ability to harvest light from both the donor and the acceptor phases in BHJs. Further examination of the charge-carrier dynamics in these systems, control of the nanoscale morphology,[194] and careful engineering of the organic−inorganic interfaces,[194,198] could improve their solar cell efficiencies while better material combinations continue to emerge.

Concurrent efforts continue to be invested in organic−inorganic hybrid configurations that rely on mesoporous oxide layers as the electron transport material (typically TiO_2), and conjugated polymers as a combined light harvesting and hole transporting material.[205,206] One of the most recent and promising solid-state device involved mesoporous TiO_2 sensitized by Sb_2S_3 with P3HT as the hole-conducting dye.[207] This configuration yielded over 5% PCE, and FFs of nearly 70%, though with a relatively modest maximum $V_{OC} \approx 0.56$ V. Device performance should be further improved by acquiring a better understanding of the charge-transport phenomena at the organic−inorganic junctions, and by identifying the most appropriate organic and inorganic components to be integrated in these architectures.

While this is beyond the scope of this report, it should be mentioned that much progress has been made in the area of solid-state dye-sensitized solar cells (ss-DSSCs) based on small-molecule sensitizing and hole-transporting materials,[208,209] affording certified PCEs in excess of 6%.[210]

BEYOND DEVICE PERFORMANCE PARAMETERS

A detailed analysis of state-of-the-art BHJ solar cells[40,43,76,211] suggests that maximizing the V_{OC} produced by these devices under illumination, while maintaining high short-circuit and photogenerated currents, is key to reaching PCEs approaching 10% and beyond. Previous studies on polymer-based BHJ solar cells have shown that the device V_{OC} scales with the difference between the HOMO energy of the donor and the LUMO energy of the acceptor (Figure 14a).[212−215] A number of more recent reports further suggest that the generated photovoltage is not only controlled by the energetics of the DA pair, but also by the saturation dark current.[216−218] The latter would be intimately connected to bulk morphology, degree of microstructural order, and intermolecular interactions.

In particular, the V_{OC} in vapor-deposited bilayer OPVs composed of C_{60} and various donors has been shown to exhibit a strong inverse dependence on the saturation dark-current density (J_S).[216] The presence of aggregation and polycrystallinity in the donor phase, as seen in thin-film absorption spectra and by X-ray diffraction, respectively, resulted in higher dark currents, hence in lower V_{OC} values. In contrast, the less ordered, more amorphous donor systems produced lower J_S and therefore higher V_{OC} values (e.g., tetracene vs rubrene, Figure 14b). A correlation between the strength of intermolecular interactions in the donor phase and the V_{OC} was drawn, and points toward the design of donor materials that do not exhibit overly pronounced intermolecular interactions. However, donors should retain relatively high carrier mobilities and exciton diffusion lengths in order to maintain high short-circuit current (J_{SC}) and FF. In parallel, systems with high optical densities and large spectral overlap should also promote high J_{SC} values. The same trends should be observable for acceptor materials,[219] and may eventually be extended to solution-processed BHJ device architectures.

The correlation between V_{OC} and dark current has been reinforced in polymer/C_{60} bilayer solar cells subjected to post-deposition thermal annealing.[217] As the donor and acceptor layers intermixed, coincident improvement in V_{OC} and reduction of J_S were observed until C_{60} fully penetrated the polymer phase and reached the ITO/PEDOT:PSS anode thus causing a reduction in V_{OC}. Under these conditions, introduction of a pentacene electron-blocking layer at the interface between ITO/PEDOT:PSS anode and photoactive heterojunction leads to a drastic increase in V_{OC} (150%) and shunt resistance ($\times 10^3$), with reduced dark current ($\div 10^3$), and improved device performance (Figure 14c). Nonetheless, the reasons for a concurrent reduction of J_{SC} observed with increasing pentacene thickness (and V_{OC}) remain to be elucidated. Considering the relatively constant FF values with varying pentacene thickness, the device PCE could be enhanced much further if J_{SC} could at least be maintained. The presence of interlayers and their effect on V_{OC}, J_{SC}, and J_S is a topic of increasing fundamental interest.[220−223] Correlations between the pattern of alkyl side chains of the polymer donor,[224] or the presence of electron-deficient units,[225] and these parameters have also been drawn.

In a subsequent contribution, the principle of detailed balance[226] was used to demonstrate that the electroluminescence (EQE_{EL}) and photovoltaic external quantum efficiencies (EQE_{PV}) in the low-energy charge-transfer spectral region of polymer/fullerene blends are connected, and that the corresponding spectra are related to V_{OC}.[218] Interestingly, EQE_{EL} spectra of DA blends are largely dominated by charge-transfer emission in contrast with EQE_{PV} spectra, and also significantly more red-shifted than the emission spectra of their separate donor and acceptor components. Empirical correlations between position of the charge-transfer bands on the electromagnetic

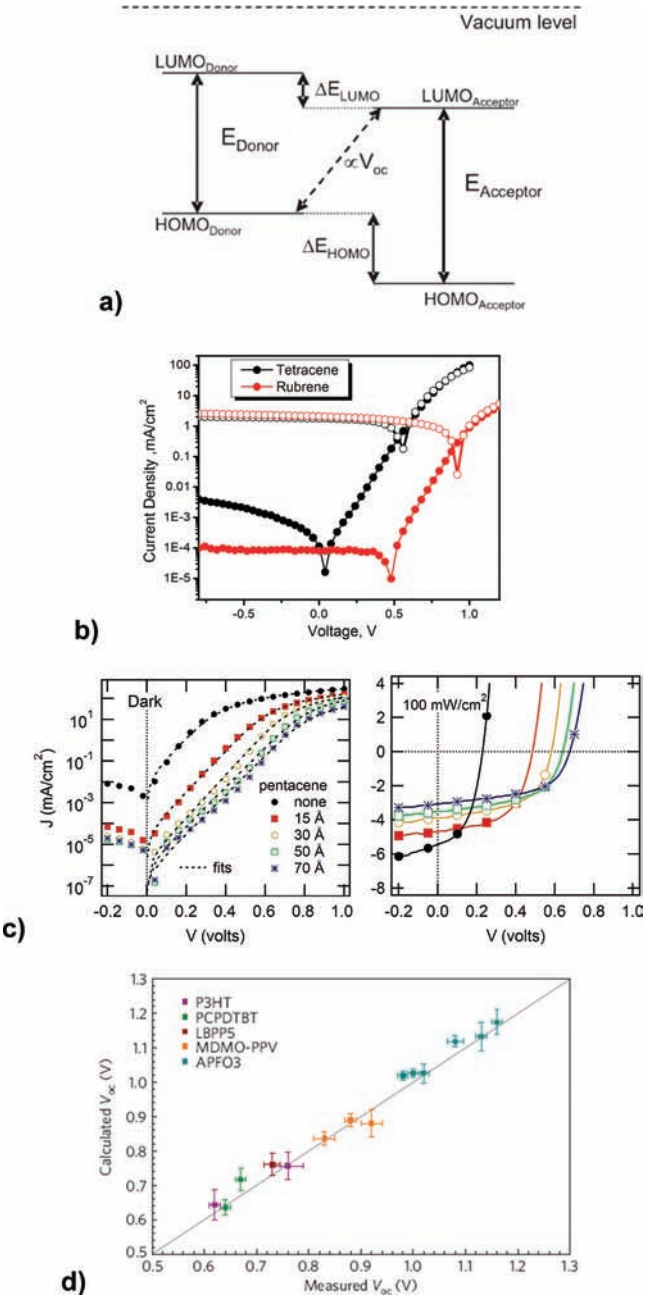

Figure 14. (a) V_{OC} roughly scales with the difference between the donor HOMO and the acceptor LUMO. Reproduced with permission from ref 85. Copyright 2009 Wiley. (b) $J-V$ characteristics in the dark (closed circles) and under illumination (open circles) in vapor-deposited tetracene- and rubrene-based bilayer OPVs with C_{60}. The V_{OC} shows a strong inverse dependence on the saturation dark current density. Reproduced with permission from ref 216. Copyright 2009 American Chemical Society. (c) A pentacene electron-blocking layer at the interface between ITO/PEDOT:PSS anode and a polymer/C_{60} bilayer heterojunction reduces dark current, and increases V_{OC} and shunt resistance. Reproduced with permission from ref 217. Copyright 2009 American Chemical Society. (d) V_{OC} obtained via the detailed balance approach vs experimental V_{OC} for various combinations of polymer donors and fullerene acceptors. This approach assumes a logarithmic dependence of V_{OC} on dark current. Reproduced with permission from ref 218. Copyright 2009 Nature Publishing Group.

spectrum and V_{OC} have been drawn in the past.[227−229] This recent report[218] reveals that a blue-shift of the charge-transfer band results in an exponential decrease of the saturated dark current. Given the logarithmic dependence of V_{OC} on dark current, it is concluded that V_{OC} depends linearly on the spectral position of the charge-transfer band; a result that rationalizes the well-established correlation between V_{OC} and the energetic difference between polymer donor HOMO and fullerene acceptor LUMO states. Figure 14d validates the use of the detailed balance approach in estimating V_{OC}. Along these lines, it is expected that an increase in V_{OC} could be achieved by employing DA systems with less pronounced electronic couplings to reduce the dark current. Considering EQE_{EL} values in the range $10^{-9}-10^{-6}$ as typical with OPV devices made from semiconducting polymer-fullerene blends,[218] and a theoretical maximum $EQE_{EL} = 1$ achieved in a system exclusively governed by radiative recombinations, another way to increase V_{OC} would involve minimizing the nonradiative recombination pathways, which could provide an increase in OPV device V_{OC} of up to 0.3−0.5 V. In this regard, inspecting the exact origin of nonradiative recombinations in OPVs should remain a target of investigation.[230,231]

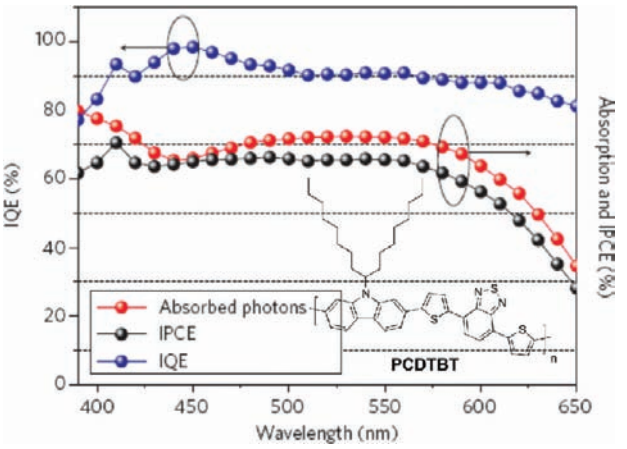

Figure 15. Internal quantum efficiency (IQE) vs wavelength (blue curve) for a BHJ solar cell made with the narrow-bandgap polymer donor PCDTBT (**29**, Chart 1) and $PC_{71}BM$ (**31**) (1:4). The overall absorption of the device (red curve), and the EQE_{PV} (black curve) are shown for comparison. Reproduced with permission from ref 76. Copyright 2009 Nature Publishing Group.

Beyond these considerations, it is worth noting that a number of energy requirements and loss mechanisms, including a minimum energy offset of 0.1 eV for charge transfer (CT) from the lowest energy singlet excited state of the donor (or acceptor) to the CT state, and 0.3 eV accounting for the Coulombic energy difference between *inter*- and *intra*molecular CT excitons, may subsist.[213] These could ultimately limit the maximum attainable V_{OC} in optimized DA blends.

Current state-of-the-art BHJ solar cells with π-conjugated polymers can exhibit EQE_{PV} values exceeding 60% over a broad range of the visible spectrum,[76] with some demonstrating remarkable internal quantum efficiencies (IQEs) that approach 100% (Figure 15). This implies that all photogenerated electron−hole pairs dissociate into free charges, which can be transported across the device without recombining, and can then be extracted.[45,76] IQE plots are typically generated by measuring overall device optical absorption and EQE_{PV}.[232−234] Considering parasitic absorptions by the contact electrodes and/or by other nonactive layers such as charge blocking layers or optical

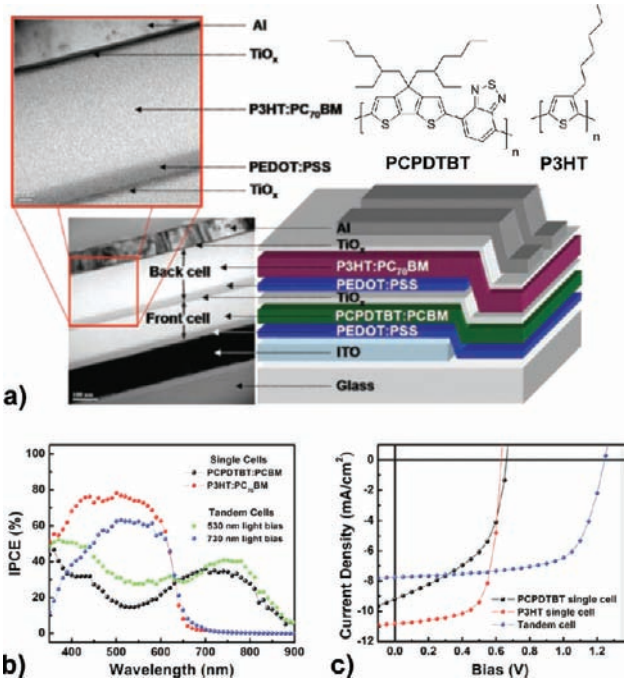

Figure 16. (a) Device structure (right) and TEM cross-sectional image (left) of a polymer tandem solar cell using P3HT (**3**) and the narrow bandgap PCPDTBT (**9**). Scale bars: 100 nm (lower image) and 20 nm (upper image). (b) EQE_{PV} (IPCE, incident photon to current conversion efficiency) spectra of single cells and the tandem cell using P3HT as the high-energy photon absorber, and the narrow bandgap PCPDTBT absorbing at longer (complementary) wavelengths, under light bias. (c) $J-V$ characteristics of the corresponding single cells and tandem cell under AM1.5G illumination. PCPDTBT:$PC_{61}BM$ single cell: J_{SC} = 9.2 mA/cm^2, V_{OC} = 0.66 V, FF = 50%, and PCE = 3.0%. P3HT:$PC_{71}BM$ single cell: J_{SC} = 10.8 mA/cm^2, V_{OC} = 0.63 V, FF = 69%, and PCE = 4.7%. Tandem cell: J_{SC} = 7.8 mA/cm^2, V_{OC} = 1.24 V, FF = 67%, and PCE = 6.5%. Reproduced with permission from ref 237. Copyright 2007 American Association for Advancement of Science.

spacers in vertically stacked OPV devices, the determination of the exact contribution of the active layer to the overall optical absorption can be somewhat challenging. In this regard, a simple approach to refining IQE measurements has been recently suggested.[235] This approach, which attempts to minimize experimental error based on the use of an optical model to calculate and subtract the parasitic absorption from the measured optical absorption of the device, could be particularly useful in providing more accurate descriptions of the charge dynamics in OPVs.

Considering the relatively low dielectric constants and high recombination rates that prevail in organic electronics, the thickness of the active layer rarely exceeds 120 nm under optimized OPV device performance conditions. At this thickness, a substantial amount of light is not absorbed by the organics and the corresponding energy is lost. In addition, the discrete absorption bands of organic semiconductors do not match the optical coverage of their inorganic counterparts, and here again a substantial amount of light is not captured. In particular, photons with sub-bandgap energy will be transmitted, and the highest-energy photons will lose their excess energy via thermal equilibration.[236]

Tandem solar cells in which several active layers are vertically stacked to maximize light-harvesting without compromising charge transport and collection at the electrodes, represent

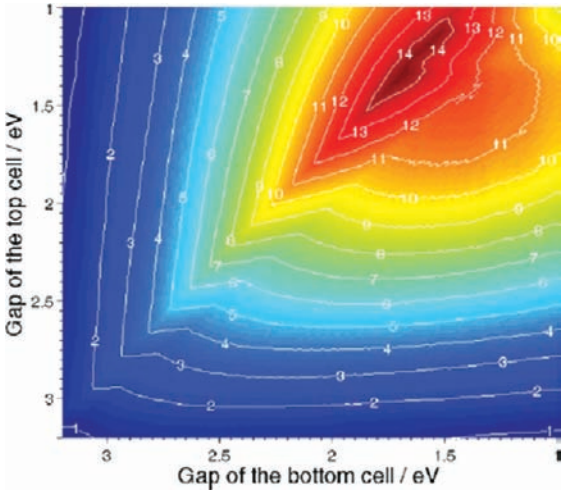

Figure 17. Predicted efficiency (PCE in %) of a tandem solar cell device composed of two polymer donors as a function of the bandgap of the two polymers incorporated. Initial assumptions for the predictions include a difference between the LUMO of the polymer donor and that of the fullerene acceptor of 0.3 eV, EQE_{PV} of the subdevices as high as (and limited to) 65%, and IQE = 85% for the bottom device. Reproduced with permission from ref 243. Copyright 2008 Wiley.

a flexible platform through the combination of materials with complementary spectral absorptions.[236−241] In an ideal configuration, the semitransparent recombination layer aligning the quasi-Fermi levels of donor and acceptor components between two subcells[85] can be solution-processed without disrupting the first junction. ZnO and TiOx are examples of recombination layer materials that can be spin-cast for the first, or deposited via sol−gel approach for the second. Interestingly, one of the highest-performing organic tandem solar cell reported to date was entirely solution-processed, involved polymeric semiconductors with complementary visible absorptions, and achieved a PCE of 6.5% under AM1.5G (Figure 16).[237] More recently, a tandem device made of a front subcell of P3HT donor and fullerene ICBA acceptor, and a rear subcell of PSBTBT and $PC_{71}BM$, reached 7% PCE.[242] A number of reports predict that PCEs approaching 15% should be attainable with organic semiconductors using the tandem junction cell approach (Figure 17).[85,243] As it is now established that the photocurrent of a tandem device can exceed that of the current-limiting subcell, matching the photocurrents of the subcells should not necessarily be considered as a determining design principle for future tandem device optimization work.[236] In contrast, the nature of the interlayer between subcells is expected to have a critical impact on device operation and overall efficiency.[239,242]

Overall, building a more fundamental understanding of the structural variables (e.g., electronics, morphology, interfaces) governing device performance parameters should provide further guidance for new material design, and help achieve optimized efficiencies with the promising systems currently being explored.

CONCLUDING REMARKS AND OUTLOOK

While BHJs of the semicrystalline polymer donor P3HT and the fullerene acceptor $PC_{61}BM$, with solar cell efficiencies of ~5%, had long represented the state-of-the-art in the field of

OPVs, a number of low-bandgap polymers containing *donor–acceptor* motifs have recently been used to achieve efficiencies approaching 10%. As a result of their narrow energy gap, these systems possess absorption spectra red-shifted in the desirable 500–800 nm wavelength region. The DA approach is also proving valuable in allowing the use of solution-processable low band gap small molecules in BHJ cells that may soon rival polymer-based cells in terms of achievable power conversion efficiency. Interestingly, both higher-performing polymeric and small-molecule systems tend to show a substantial degree of nanostructural order in thin-film devices, despite the apparent lack of long-range order and extended crystallinity observed in several instances. This is also the case in polymeric OTFTs where low-bandgap materials have recently been used to achieve electron mobilities approaching 1 $cm^2\ V^{-1}\ s^{-1}$ and hole mobilities exceeding 1 $cm^2\ V^{-1}\ s^{-1}$, thus showing charge-transport properties comparable to those achievable with their more crystalline small-molecule counterparts. Building on earlier work with vapor-deposited and single-crystal small-molecule OTFTs achieving carrier mobilities in the range of 1–20 $cm^2\ V^{-1}\ s^{-1}$, it is plausible that mobilities exceeding 10 $cm^2\ V^{-1}\ s^{-1}$ can be reached with polymers upon incorporating long and planar polycyclic aromatic building blocks with appropriate solubilizing side chains. In highly crystalline small-molecule thin films, the transport of charge carriers remains inherently limited by the grain boundaries that segregate crystallites with distinct relative orientations. In these systems, strategies aimed at improving the interconnection between crystallites should lead to enhanced charge-carrier transport. On this basis, the same strategies could also help reduce the charge recombination rates and improve FFs in small-molecule BHJ solar cells.

It is likely that alternative DA motifs can be found to improve the spectral coverage and absorption coefficients of small molecules for OPV applications, thus increasing J_{SC}. As with polymers, the incorporation of nanoparticles with localized surface plasmon resonances in the active layer could ultimately allow concentrating light within the BHJ.[244] In parallel, more effective strategies to increase the optical paths in the active layer, for example by scattering light, may also provide for enhanced light absorption. Overall, the full potential of inorganic nanoparticles in organic BHJs remains to be explored, including the possibility for these to act as effective electron-donor or electron-acceptor semiconducting components in hybrid BHJs. A worthwhile target would involve tailoring the interface between organic and inorganic materials in order to achieve more effective cooperative electronic interactions and more intimate blend morphologies.

Finding synthetically accessible alternatives to the electron-acceptor PCBM, while maintaining both highly efficient electron-transport properties and the ability to phase separate in relatively ordered domains, would have a great impact on the development of organic solar cells, and ultimately their commercial viability. This is an area where a breakthrough in the development of high-performing electron-deficient polymers could provide new perspectives.

The panel of analytical techniques from which fundamental insight into the structure–property relationships of semiconducting polymers can be obtained was recently reviewed in a comprehensive article with emphasis on thin-film microstructural characterization.[245] Since charge-carrier generation and transport efficiency in organic electronics are intimately related to nanoscale morphology and microstructural order, important correlations between molecular structure and material properties can generally be drawn from a feedback loop of material design, device testing, and thin-film characterization. Nonetheless, a number of challenges related to the modest dielectric constants, small exciton diffusion lengths, and limited carrier mobilities inherent to organic electronics remain to be tackled. These challenges may entail the development and implementation of strategies for structuring the nanoscale morphology of thin-film devices as well as examining charge transport at a nanoscopic level. Once optimized processing or postprocessing conditions and morphologies are identified, efficient approaches enabling the immobilization of the nanostructural architecture of the active layer will need to be applied in order to prevent further crystallization and demixing events from occurring with time and temperature fluctuations. Further device reliability studies should confirm whether such strategies can provide access to stable and durable device properties, which are comparable to those now routinely achieved with their inorganic counterparts.

It is obvious that translating the material and system performance parameters obtained in laboratory-scale devices to large-area devices solution-processed via roll-to-roll or other high-throughput printing techniques raises a new challenge. This is an area where a growing amount of research carried out in parallel in academia and industry is aimed at a demonstration of the commercial viability of organic electronics for application in circuit logics as well as solar power-generating technologies.[23,85,109,246,247] Ultimately, with the development of new materials, interlayers and optimized device configurations, all-solution-processed organic tandem solar cells may eventually rival inorganic-based cells, such as those based on *a*-Si, CdTe, and $Cu(In,Ga)Se_2$, in terms of achievable PCE and for a large range of portable device applications.

A number of comprehensive articles and reviews describing material design and device aspects, as applied to OPVs and to OTFTs, have been published in recent years. A number of these have emphasized material design,[128,129,143,144,152,166,187,248–257] thin-film structural order,[26,46,258] device strategies[85,259,260] and physics,[80,261] tandem architectures,[240,241] quantum chemical calculations,[189,262] device stability,[246,260] or economical aspects.[85] This concise Perspective providing a critical review and evaluation of a number of recently suggested approaches toward the design and structural organization of π-functional materials should complement the breadth of existing literature in these fast-developing areas.

■ ASSOCIATED CONTENT

Supporting Information. Complete refs 25, 60, 116, 124, and 246. This material is available free of charge via the Internet at http://pubs.acs.org.

■ AUTHOR INFORMATION

Corresponding Author
pierre.beaujuge@kaust.edu.sa; jean.frechet@kaust.edu.sa

■ ACKNOWLEDGMENT

The authors acknowledge the financial support of the "Plastics Electronics" program at Lawrence Berkeley National Laboratory

by the Director, Office of Science, Office of Basic Energy Sciences, Materials Sciences and Engineering Division, of the U.S. Department of Energy under Contract No. DE-AC02-05CH11231. Additional support under the CAMP-KAUST program funded by King Abdullah University of Science and Technology is also acknowledged with thanks. The authors thank Dr. Claire Woo for helpful discussions and useful scientific insight.

REFERENCES

(1) Zhang, M.; Tsao, H. N.; Pisula, W.; Yang, C.; Mishra, A. K.; Müllen, K. *J. Am. Chem. Soc.* **2007**, *129*, 3472.
(2) Wu, J.; Pisula, W.; Müllen, K. *Chem. Rev.* **2007**, *107*, 718.
(3) Grevin, B.; Rannou, P.; Payerne, R.; Pron, A.; Travers, J. P. J. Chem. Phys. **2003**, *118*, 7097.
(4) Zhang, R.; Li, B.; Iovu, M. C.; Jeffries-El, M.; Sauvé, G.; Cooper, J.; Jia, S.; Tristram-Nagle, S.; Smilgies, D. M.; Lambeth, D. N.; McCullough, R. D.; Kowalewski, T. *J. Am. Chem. Soc.* **2006**, *128*, 3480.
(5) Ma, W.; Yang, C.; Gong, X.; Lee, K.; Heeger, A. J. *Adv. Funct. Mater.* **2005**, *15*, 1617.
(6) Li, G.; Shrotriya, V.; Huang, J.; Yao, Y.; Moriarty, T.; Emery, K.; Yang, Y. *Nat. Mater.* **2005**, *4*, 864.
(7) Gadisa, A.; Oosterbaan, W. D.; Vandewal, K.; Bolsée, J.-C.; Bertho, S.; D'Haen, J.; Lutsen, L.; Vanderzande, D.; Manca, J. V. *Adv. Funct. Mater.* **2009**, *19*, 3300.
(8) Nguyen, L. H.; Hoppe, H.; Erb, T.; Günes, S.; Gobsch, G.; Sariciftci, N. S. *Adv. Funct. Mater.* **2007**, *17*, 1071.
(9) Campoy-Quiles, M.; Ferenczi, T.; Agostinelli, T.; Etchegoin, P. G.; Kim, Y.; Anthopoulos, T. D.; Stavrinou, P. N.; Bradley, D. D. C.; Nelson, J. *Nat. Mater.* **2008**, *7*, 158.
(10) Chen, D.; Nakahara, A.; Wei, D.; Nordlund, D.; Russell, T. P. *Nano Lett.* **2010**, *11*, 561.
(11) Jimison, L. H.; Toney, M. F.; McCulloch, I.; Heeney, M.; Salleo, A. *Adv. Mater.* **2009**, *21*, 1568.
(12) Kim, Y.; Cook, S.; Tuladhar, S. M.; Choulis, S. A.; Nelson, J.; Durrant, J. R.; Bradley, D. D. C.; Giles, M.; McCulloch, I.; Ha, C.-S.; Ree, M. *Nat. Mater.* **2006**, *5*, 197.
(13) Thompson, B. C.; Kim, B. J.; Kavulak, D. F.; Sivula, K.; Mauldin, C.; Fréchet, J. M. J. *Macromolecules* **2007**, *40*, 7425.
(14) Sivula, K.; Luscombe, C. K.; Thompson, B. C.; Fréchet, J. M. J. *J. Am. Chem. Soc.* **2006**, *128*, 13988.
(15) Woo, C. H.; Thompson, B. C.; Kim, B. J.; Toney, M. F.; Fréchet, J. M. J. *J. Am. Chem. Soc.* **2008**, *130*, 16324.
(16) Oosterbaan, W. D.; Vrindts, V.; Berson, S.; Guillerez, S.; Douheret, O.; Ruttens, B.; D'Haen, J.; Adriaensens, P.; Manca, J.; Lutsen, L.; Vanderzande, D. *J. Mater. Chem.* **2009**, *19*, 5424.
(17) Kline, R. J.; McGehee, M. D.; Kadnikova, E. N.; Liu, J.; Fréchet, J. M. J. *Adv. Mater.* **2003**, *15*, 1519.
(18) Ballantyne, A. M.; Chen, L.; Dane, J.; Hammant, T.; Braun, F. M.; Heeney, M.; Duffy, W.; McCulloch, I.; Bradley, D. D. C.; Nelson, J. *Adv. Funct. Mater.* **2008**, *18*, 2373.
(19) Koppe, M.; Brabec, C. J.; Heiml, S.; Schausberger, A.; Duffy, W.; Heeney, M.; McCulloch, I. *Macromolecules* **2009**, *42*, 4661.
(20) Singh, K. A.; Sauve, G.; Zhang, R.; Kowalewski, T.; McCullough, R. D.; Porter, L. M. *Appl. Phys. Lett.* **2008**, *92*, 263303.
(21) Zen, A.; Pflaum, J.; Hirschmann, S.; Zhuang, W.; Jaiser, F.; Asawapirom, U.; Rabe, J. P.; Scherf, U.; Neher, D. *Adv. Funct. Mater.* **2004**, *14*, 757.
(22) Kline, R. J.; McGehee, M. D.; Kadnikova, E. N.; Liu, J.; Fréchet, J. M. J.; Toney, M. F. *Macromolecules* **2005**, *38*, 3312.
(23) McCulloch, I.; Heeney, M.; Bailey, C.; Genevicius, K.; MacDonald, I.; Shkunov, M.; Sparrowe, D.; Tierney, S.; Wagner, R.; Zhang, W.; Chabinyc, M. L.; Kline, R. J.; McGehee, M. D.; Toney, M. F. *Nat. Mater.* **2006**, *5*, 328.
(24) DeLongchamp, D. M.; Kline, R. J.; Lin, E. K.; Fischer, D. A.; Richter, L. J.; Lucas, L. A.; Heeney, M.; McCulloch, I.; Northrup, J. E. *Adv. Mater.* **2007**, *19*, 833.
(25) McCulloch, I.; et al. *Adv. Mater.* **2009**, *21*, 1091.
(26) Wang, C.; Jimison, L. H.; Goris, L.; McCulloch, I.; Heeney, M.; Ziegler, A.; Salleo, A. *Adv. Mater.* **2010**, *22*, 697.
(27) Zhang, X.; Hudson, S. D.; DeLongchamp, D. M.; Gundlach, D. J.; Heeney, M.; McCulloch, I. *Adv. Funct. Mater.* **2010**, *20*, 4098.
(28) Liu, J.; Zhang, R.; Sauvé, G.; Kowalewski, T.; McCullough, R. D. *J. Am. Chem. Soc.* **2008**, *130*, 13167.
(29) Liu, J.; Zhang, R.; Osaka, I.; Mishra, S.; Javier, A. E.; Smilgies, D. M.; Kowalewski, T.; McCullough, R. D. *Adv. Funct. Mater.* **2009**, *19*, 3427.
(30) Osaka, I.; Sauvé, G.; Zhang, R.; Kowalewski, T.; McCullough, R. D. *Adv. Mater.* **2007**, *19*, 4160.
(31) Osaka, I.; Zhang, R.; Sauvé, G.; Smilgies, D.-M.; Kowalewski, T.; McCullough, R. D. *J. Am. Chem. Soc.* **2009**, *131*, 2521.
(32) Osaka, I.; Zhang, R.; Liu, J.; Smilgies, D.-M.; Kowalewski, T.; McCullough, R. D. *Chem. Mater.* **2010**, *22*, 4191.
(33) Havinga, E. E.; Hoeve, W.; Wynberg, H. *Polym. Bull.* **1992**, *29*, 119.
(34) Havinga, E. E.; Hoeve, W.; Wynberg, H. *Synth. Met.* **1993**, *55*, 299.
(35) Tsao, H. N.; Cho, D.; Andreasen, J. W.; Rouhanipour, A.; Breiby, D. W.; Pisula, W.; Müllen, K. *Adv. Mater.* **2009**, *21*, 209.
(36) Tsao, H. N.; Cho, D. M.; Park, I.; Hansen, M. R.; Mavrinskiy, A.; Yoon, D. Y.; Graf, R.; Pisula, W.; Spiess, H. W.; Müllen, K. *J. Am. Chem. Soc.* **2011**, *133*, 2605.
(37) Hsiang-Yu, C.; Jianhui, H.; Amy, E. H.; Hoichang, Y.; Houk, K. N.; Yang, Y. *Adv. Mater.* **2010**, *22*, 371.
(38) Scharber, M. C.; Koppe, M.; Gao, J.; Cordella, F.; Loi, M. A.; Denk, P.; Morana, M.; Egelhaaf, H.-J.; Forberich, K.; Dennler, G.; Gaudiana, R.; Waller, D.; Zhu, Z.; Shi, X.; Brabec, C. J. *Adv. Mater.* **2010**, *22*, 367.
(39) Hou, J.; Chen, H.-Y.; Zhang, S.; Li, G.; Yang, Y. *J. Am. Chem. Soc.* **2008**, *130*, 16144.
(40) Piliego, C.; Holcombe, T. W.; Douglas, J. D.; Woo, C. H.; Beaujuge, P. M.; Fréchet, J. M. J. *J. Am. Chem. Soc.* **2010**, *132*, 7595.
(41) Liang, Y.; Wu, Y.; Feng, D.; Tsai, S.-T.; Son, H.-J.; Li, G.; Yu, L. *J. Am. Chem. Soc.* **2008**, *131*, 56.
(42) Liang, Y.; Feng, D.; Wu, Y.; Tsai, S.-T.; Li, G.; Ray, C.; Yu, L. *J. Am. Chem. Soc.* **2009**, *131*, 7792.
(43) Chen, H.-Y.; Hou, J.; Zhang, S.; Liang, Y.; Yang, G.; Yang, Y.; Yu, L.; Wu, Y.; Li, G. *Nat. Photon.* **2009**, *3*, 649.
(44) Guo, J.; Liang, Y.; Szarko, J.; Lee, B.; Son, H. J.; Rolczynski, B. S.; Yu, L.; Chen, L. X. *J. Phys. Chem. B* **2010**, *114*, 742.
(45) Liang, Y.; Xu, Z.; Xia, J.; Tsai, S.-T.; Wu, Y.; Li, G.; Ray, C.; Yu, L. *Adv. Mater.* **2010**, *22*, E135.
(46) Tsao, H. N.; Müllen, K. *Chem. Soc. Rev.* **2010**, *39*, 2372.
(47) Street, R. A.; Northrup, J. E.; Salleo, A. *Phys. Rev. B* **2005**, *71*, 165202.
(48) Beaujuge, P. M.; Pisula, W.; Tsao, H. N.; Ellinger, S.; Müllen, K.; Reynolds, J. R. *J. Am. Chem. Soc.* **2009**, *131*, 7514.
(49) Baker, J. L.; Jimison, L. H.; Mannsfeld, S.; Volkman, S.; Yin, S.; Subramanian, V.; Salleo, A.; Alivisatos, A. P.; Toney, M. F. *Langmuir* **2010**, *26*, 9146.
(50) Price, S. C.; Stuart, A. C.; Yang, L.; Zhou, H.; You, W. *J. Am. Chem. Soc.* **2011**, *133*, 4625.
(51) Son, H. J.; Wang, W.; Xu, T.; Liang, Y.; Wu, Y.; Li, G.; Yu, L. *J. Am. Chem. Soc.* **2011**, *133*, 1885.
(52) Tong, M.; Cho, S.; Rogers, J. T.; Schmidt, K.; Hsu, B. B. Y.; Moses, D.; Coffin, R. C.; Kramer, E. J.; Bazan, G. C.; Heeger, A. J. *Adv. Funct. Mater.* **2010**, *20*, 3959.
(53) Coffin, R. C.; Peet, J.; Rogers, J.; Bazan, G. C. *Nat. Chem.* **2009**, *1*, 657.
(54) Bijleveld, J. C.; Zoombelt, A. P.; Mathijssen, S. G. J.; Wienk, M. M.; Turbiez, M.; de Leeuw, D. M.; Janssen, R. A. J. *J. Am. Chem. Soc.* **2009**, *131*, 16616.
(55) Müller, C.; Wang, E.; Andersson, L. M.; Tvingstedt, K.; Zhou, Y.; Andersson, M. R.; Inganäs, O. *Adv. Funct. Mater.* **2010**, *20*, 2124.
(56) Park, J. K.; Jo, J.; Seo, J. H.; Moon, J. S.; Park, Y. D.; Lee, K.; Heeger, A. J.; Bazan, G. C. *Adv. Mater.* **2011**, *23*, 2430.

(57) Liang, Y.; Yu, L. *Acc. Chem. Res.* **2010**, *43*, 1227.
(58) Zou, Y.; Najari, A.; Berrouard, P.; Beaupré, S.; Réda Aich, B.; Tao, Y.; Leclerc, M. *J. Am. Chem. Soc.* **2010**, *132*, 5330.
(59) Zhang, Y.; Hau, S. K.; Yip, H.-L.; Sun, Y.; Acton, O.; Jen, A. K. Y. *Chem. Mater.* **2010**, *22*, 2696.
(60) Bronstein, H.; et al. *J. Am. Chem. Soc.* **2011**, *133*, 3272.
(61) Meredig, B.; Salleo, A.; Gee, R. *ACS Nano* **2009**, *3*, 2881.
(62) Wienk, M. M.; Turbiez, M.; Janssen, R. A. J. *Adv. Mater.* **2008**, *20*, 2556.
(63) Peet, J.; Heeger, A. J.; Bazan, G. C. *Acc. Chem. Res.* **2009**, *42*, 1700.
(64) Peet, J.; Kim, J. Y.; Coates, N. E.; Ma, W. L.; Moses, D.; Heeger, A. J.; Bazan, G. C. *Nat. Mater.* **2007**, *6*, 497.
(65) Lee, J. K.; Ma, W. L.; Brabec, C. J.; Yuen, J.; Moon, J. S.; Kim, J. Y.; Lee, K.; Bazan, G. C.; Heeger, A. J. *J. Am. Chem. Soc.* **2008**, *130*, 3619.
(66) Hoven, C. V.; Dang, X.-D.; Coffin, R. C.; Peet, J.; Nguyen, T.-Q.; Bazan, G. C. *Adv. Mater.* **2010**, *22*, E63.
(67) Caputo, B. J. A.; Welch, G. C.; Kamkar, D. A.; Henson, Z. B.; Nguyen, T.-Q.; Bazan, G. C. *Small* **2011**, *7*, 1422.
(68) Rogers, J. T.; Schmidt, K.; Toney, M. F.; Kramer, E. J.; Bazan, G. C. *Adv. Mater.* **2011**, *23*, 2284.
(69) Moon, J. S.; Takacs, C. J.; Cho, S.; Coffin, R. C.; Kim, H.; Bazan, G. C.; Heeger, A. J. *Nano Lett.* **2010**, *10*, 4005.
(70) Chu, T.-Y.; Lu, J.; Beaupré, S.; Zhang, Y.; Pouliot, J.-R.; Wakim, S.; Zhou, J.; Leclerc, M.; Li, Z.; Ding, J.; Tao, Y. *J. Am. Chem. Soc.* **2011**, *133*, 4250.
(71) Amb, C. M.; Chen, S.; Graham, K. R.; Subbiah, J.; Small, C. E.; So, F.; Reynolds, J. R. *J. Am. Chem. Soc.* **2011**, *133*, 10062.
(72) Zhang, Y.; Zou, J.; Yip, H.-L.; Sun, Y.; Davies, J. A.; Chen, K.-S.; Acton, O.; Jen, A. K. Y. *J. Mater. Chem.* **2011**, *21*, 3895.
(73) Maturová, K.; van Bavel, S. S.; Wienk, M. M.; Janssen, R. A. J.; Kemerink, M. *Adv. Funct. Mater.* **2011**, *21*, 261.
(74) Morana, M.; Azimi, H.; Dennler, G.; Egelhaaf, H.-J.; Scharber, M.; Forberich, K.; Hauch, J.; Gaudiana, R.; Waller, D.; Zhu, Z.; Hingerl, K.; van Bavel, S. S.; Loos, J.; Brabec, C. J. *Adv. Funct. Mater.* **2010**, *20*, 1180.
(75) Cates, N. C.; Gysel, R.; Beiley, Z.; Miller, C. E.; Toney, M. F.; Heeney, M.; McCulloch, I.; McGehee, M. D. *Nano Lett.* **2009**, *9*, 4153.
(76) Park, S. H.; Roy, A.; Beaupre, S.; Cho, S.; Coates, N.; Moon, J. S.; Moses, D.; Leclerc, M.; Lee, K.; Heeger, A. J. *Nat. Photon.* **2009**, *3*, 297.
(77) Beaujuge, P. M.; Subbiah, J.; Choudhury, K. R.; Ellinger, S.; McCarley, T. D.; So, F.; Reynolds, J. R. *Chem. Mater.* **2009**, *22*, 2093.
(78) Blouin, N.; Michaud, A.; Gendron, D.; Wakim, S.; Blair, E.; Neagu-Plesu, R.; Belletete, M.; Durocher, G.; Tao, Y.; Leclerc, M. *J. Am. Chem. Soc.* **2007**, *130*, 732.
(79) Melzer, C.; Koop, E. J.; Mihailetchi, V. D.; Blom, P. W. M. *Adv. Funct. Mater.* **2004**, *14*, 865.
(80) Blom, P. W. M.; Mihailetchi, V. D.; Koster, L. J. A.; Markov, D. E. *Adv. Mater.* **2007**, *19*, 1551.
(81) Parmer, J., E.; Mayer, A., C.; Hardin, B., E.; Scully, S., R.; McGehee, M., D.; Heeney, M.; McCulloch, I. *Appl. Phys. Lett.* **2008**, *92*, 113309.
(82) Wang, D. H.; Moon, J. S.; Seifter, J.; Jo, J.; Park, J. H.; Park, O. K.; Heeger, A. J. *Nano Lett.* **2011**, *11*, 3163.
(83) Treat, N. D.; Brady, M. A.; Smith, G.; Toney, M. F.; Kramer, E. J.; Hawker, C. J.; Chabinyc, M. L. *Adv. Energy Mater.* **2011**, *1*, 82.
(84) Peet, J.; Wen, L.; Byrne, P.; Rodman, S.; Forberich, K.; Shao, Y.; Drolet, N.; Gaudiana, R.; Dennler, G.; Waller, D. *Appl. Phys. Lett.* **2011**, *98*, 043301.
(85) Dennler, G.; Scharber, M. C.; Brabec, C. J. *Adv. Mater.* **2009**, *21*, 1323.
(86) Wang, E.; Hou, L.; Wang, Z.; Hellström, S.; Zhang, F.; Inganäs, O.; Andersson, M. R. *Adv. Mater.* **2010**, *22*, 5240.
(87) Keivanidis, P. E.; Laquai, F.; Howard, I. A.; Friend, R. H. *Adv. Funct. Mater.* **2011**, *21*, 1355.
(88) Kim, B. J.; Miyamoto, Y.; Ma, B.; Fréchet, J. M. J. *Adv. Funct. Mater.* **2009**, *19*, 2273.
(89) Agostinelli, T.; Lilliu, S.; Labram, J. G.; Campoy-Quiles, M.; Hampton, M.; Pires, E.; Rawle, J.; Bikondoa, O.; Bradley, D. D. C.; Anthopoulos, T. D.; Nelson, J.; Macdonald, J. E. *Adv. Funct. Mater.* **2011**, *21*, 1701.
(90) Miyanishi, S.; Tajima, K.; Hashimoto, K. *Macromolecules* **2009**, *42*, 1610.
(91) Png, R.-Q.; Chia, P.-J.; Tang, J.-C.; Liu, B.; Sivaramakrishnan, S.; Zhou, M.; Khong, S.-H.; Chan, H. S. O.; Burroughes, J. H.; Chua, L.-L.; Friend, R. H.; Ho, P. K. H. *Nat. Mater.* **2010**, *9*, 152.
(92) Muller, C. D.; Falcou, A.; Reckefuss, N.; Rojahn, M.; Wiederhirn, V.; Rudati, P.; Frohne, H.; Nuyken, O.; Becker, H.; Meerholz, K. *Nature* **2003**, *421*, 829.
(93) Solomeshch, O.; Yu, Y.-J.; Medvedev, V.; Razin, A.; Blumer-Ganon, B.; Eichen, Y.; Jin, J.-I.; Tessler, N. *Synth. Met.* **2007**, *157*, 841.
(94) Charas, A.; Alves, H.; Martinho, J. M. G.; Alcácer, L.; Fenwick, O.; Cacialli, F.; Morgado, J. *Synth. Met.* **2008**, *158*, 643.
(95) Cheng, Y.-J.; Liu, M. S.; Zhang, Y.; Niu, Y.; Huang, F.; Ka, J.-W.; Yip, H.-L.; Tian, Y.; Jen, A. K. Y. *Chem. Mater.* **2007**, *20*, 413.
(96) Klarner, G.; Lee, J. I.; Lee, V. Y.; Chan, E.; Chen, J. P.; Nelson, A.; Markiewicz, D.; Siemens, R.; Scott, J. C.; Miller, R. D. *Chem. Mater.* **1999**, *11*, 1800.
(97) Halls, J. J. M.; Walsh, C. A.; Greenham, N. C.; Marseglia, E. A.; Friend, R. H.; Moratti, S. C.; Holmes, A. B. *Nature* **1995**, *376*, 498.
(98) Yu, G.; Heeger, A. J. *J. Appl. Phys.* **1995**, *78*, 4510.
(99) Moore, J. R.; Albert-Seifried, S.; Rao, A.; Massip, S.; Watts, B.; Morgan, D. J.; Friend, R. H.; McNeill, C. R.; Sirringhaus, H. *Adv. Energy Mater.* **2011**, *1*, 230.
(100) Falzon, M.-F.; Wienk, M. M.; Janssen, R. A. J. *J. Phys. Chem. C* **2011**, *115*, 3178.
(101) Falzon, M.-F.; Zoombelt, A. P.; Wienk, M. M.; Janssen, R. A. J. *Phys. Chem. Chem. Phys.* **2011**, *13*, 8931.
(102) Granstrom, M.; Petritsch, K.; Arias, A. C.; Lux, A.; Andersson, M. R.; Friend, R. H. *Nature* **1998**, *395*, 257.
(103) Holcombe, T. W.; Woo, C. H.; Kavulak, D. F. J.; Thompson, B. C.; Fréchet, J. M. J. *J. Am. Chem. Soc.* **2009**, *131*, 14160.
(104) He, X.; Gao, F.; Tu, G.; Hasko, D.; Hu̇ttner, S.; Steiner, U.; Greenham, N. C.; Friend, R. H.; Huck, W. T. S. *Nano Lett.* **2010**, *10*, 1302.
(105) He, X.; Gao, F.; Tu, G.; Hasko, D. G.; Hüttner, S.; Greenham, N. C.; Steiner, U.; Friend, R. H.; Huck, W. T. S. *Adv. Funct. Mater.* **2011**, *21*, 139.
(106) Kim, Y.; Cook, S.; Choulis, S. A.; Nelson, J.; Durrant, J. R.; Bradley, D. D. C. *Chem. Mater.* **2004**, *16*, 4812.
(107) McNeill, C. R.; Abrusci, A.; Zaumseil, J.; Wilson, R.; McKiernan, M. J.; Burroughes, J. H.; Halls, J. J. M.; Greenham, N. C.; Friend, R. H. *Appl. Phys. Lett.* **2007**, *90*, 193506.
(108) Chen, Z.; Zheng, Y.; Yan, H.; Facchetti, A. *J. Am. Chem. Soc.* **2009**, *131*, 8.
(109) Yan, H.; Chen, Z.; Zheng, Y.; Newman, C.; Quinn, J. R.; Dotz, F.; Kastler, M.; Facchetti, A. *Nature* **2009**, *457*, 679.
(110) Rivnay, J.; Toney, M. F.; Zheng, Y.; Kauvar, I. V.; Chen, Z.; Wagner, V.; Facchetti, A.; Salleo, A. *Adv. Mater.* **2010**, *22*, 4359.
(111) Zhang, W.; Smith, J.; Watkins, S. E.; Gysel, R.; McGehee, M.; Salleo, A.; Kirkpatrick, J.; Ashraf, S.; Anthopoulos, T.; Heeney, M.; McCulloch, I. *J. Am. Chem. Soc.* **2010**, *132*, 11437.
(112) Rivnay, J.; Steyrleuthner, R.; Jimison, L. H.; Casadei, A.; Chen, Z.; Toney, M. F.; Facchetti, A.; Neher, D.; Salleo, A. *Macromolecules* **2011**, *44*, 5246.
(113) Lee, J.-K.; Gwinner, M. C.; Berger, R.; Newby, C.; Zentel, R.; Friend, R. H.; Sirringhaus, H.; Ober, C. K. *J. Am. Chem. Soc.* **2011**, *133*, 9949.
(114) Heeney, M.; Zhang, W.; Crouch, D. J.; Chabinyc, M. L.; Gordeyev, S.; Hamilton, R.; Higgins, S. J.; McCulloch, I.; Skabara, P. J.; Sparrowe, D.; Tierney, S. *Chem. Commun.* **2007**, 5061.
(115) Ballantyne, A. M.; Chen, L.; Nelson, J.; Bradley, D. D. C.; Astuti, Y.; Maurano, A.; Shuttle, C. G.; Durrant, J. R.; Heeney, M.; Duffy, W.; McCulloch, I. *Adv. Mater.* **2007**, *19*, 4544.

(116) Ballantyne, A. M.; et al. *Macromolecules* **2010**, *43*, 1169.
(117) Clarke, T. M.; Ballantyne, A. M.; Tierney, S.; Heeney, M.; Duffy, W.; McCulloch, I.; Nelson, J.; Durrant, J. R. *J. Phys. Chem. C* **2010**, *114*, 8068.
(118) Chen, Z.; Lemke, H.; Albert-Seifried, S.; Caironi, M.; Nielsen, M. M.; Heeney, M.; Zhang, W.; McCulloch, I.; Sirringhaus, H. *Adv. Mater.* **2010**, *22*, 2371.
(119) Mishra, S. P.; Javier, A. E.; Zhang, R.; Liu, J.; Belot, J. A.; Osaka, I.; McCullough, R. D. *J. Mater. Chem.* **2011**, *21*, 1551.
(120) Hollinger, J.; Jahnke, A. A.; Coombs, N.; Seferos, D. S. *J. Am. Chem. Soc.* **2010**, *132*, 8546.
(121) Bunz, U. H. F. *Angew. Chem., Int. Ed.* **2010**, *49*, 5037.
(122) Woo, C. H.; Beaujuge, P. M.; Holcombe, T. W.; Lee, O. P.; Fréchet, J. M. J. *J. Am. Chem. Soc.* **2010**, *132*, 15547.
(123) Bijleveld, J. C.; Karsten, B. P.; Mathijssen, S. G. J.; Wienk, M. M.; de Leeuw, D. M.; Janssen, R. A. J. *J. Mater. Chem.* **2011**, *21*, 1600.
(124) Gundlach, D. J.; et al. *Nat. Mater.* **2008**, *7*, 216.
(125) Amassian, A.; Pozdin, V. A.; Li, R.; Smilgies, D.-M.; Malliaras, G. G. *J. Mater. Chem.* **2010**, *20*, 2623.
(126) Ling, M. M.; Bao, Z. *Chem. Mater.* **2004**, *16*, 4824.
(127) Minemawari, H.; Yamada, T.; Matsui, H.; Tsutsumi, J. y.; Haas, S.; Chiba, R.; Kumai, R.; Hasegawa, T. *Nature* **2011**, *475*, 364.
(128) Murphy, A. R.; Fréchet, J. M. J. *Chem. Rev.* **2007**, *107*, 1066.
(129) Allard, S.; Forster, M.; Souharce, B.; Thiem, H.; Scherf, U. *Angew. Chem., Int. Ed.* **2008**, *47*, 4070.
(130) Mishra, A.; Ma, C.-Q.; Bauerle, P. *Chem. Rev.* **2009**, *109*, 1141.
(131) Walker, B.; Tamayo, A., B.; Dang, X.-D.; Zalar, P.; Seo, J. H.; Garcia, A.; Tantiwiwat, M.; Nguyen, T.-Q. *Adv. Funct. Mater.* **2009**, *19*, 3063.
(132) Zhang, Y.; Dang, X.-D.; Kim, C.; Nguyen, T.-Q. *Adv. Energy Mater.* **2011**, *1*, 610.
(133) Loser, S.; Bruns, C. J.; Miyauchi, H.; Ortiz, R. P.; Facchetti, A.; Stupp, S. I.; Marks, T. J. *J. Am. Chem. Soc.* **2011**, *133*, 8142.
(134) Peet, J.; Tamayo, A. B.; Dang, X. D.; Seo, J. H.; Nguyen, T. Q. *Appl. Phys. Lett.* **2008**, *93*, 163306.
(135) Tamayo, A. B.; Walker, B.; Nguyen, T.-Q. *J. Phys. Chem. C* **2008**, *112*, 11545.
(136) Tantiwiwat, M.; Tamayo, A.; Luu, N.; Dang, X.-D.; Nguyen, T.-Q. *J. Phys. Chem. C* **2008**, *112*, 17402.
(137) Tamayo, A. B.; Dang, X.-D.; Walker, B.; Seo, J.; Kent, T.; Nguyen, T.-Q. *Appl. Phys. Lett.* **2009**, *94*, 103301.
(138) Mazzio, K. A.; Yuan, M.; Okamoto, K.; Luscombe, C. K. *ACS Appl. Mater. Interfaces* **2011**, *3*, 271.
(139) Liu, Y.; Wan, X.; Yin, B.; Zhou, J.; Long, G.; Yin, S.; Chen, Y. *J. Mater. Chem.* **2010**, *20*, 2464.
(140) Graham, K. R.; Mei, J.; Stalder, R.; Shim, J. W.; Cheun, H.; Steffy, F.; So, F.; Kippelen, B.; Reynolds, J. R. *ACS Appl. Mater. Interfaces* **2011**, *3*, 1210.
(141) Burckstummer, H.; Kronenberg, N. M.; Gsanger, M.; Stolte, M.; Meerholz, K.; Wurthner, F. *J. Mater. Chem.* **2010**, *20*, 240.
(142) Rousseau, T.; Cravino, A.; Ripaud, E.; Leriche, P.; Rihn, S.; De Nicola, A.; Ziessel, R.; Roncali, J. *Chem. Commun.* **2010**, *46*, 5082.
(143) Roncali, J. *Acc. Chem. Res.* **2009**, *42*, 1719.
(144) Lloyd, M. T.; Anthony, J. E.; Malliaras, G. G. *Mater. Today* **2007**, *10*, 34.
(145) Lloyd, M. T.; Mayer, A. C.; Subramanian, S.; Mourey, D. A.; Herman, D. J.; Bapat, A. V.; Anthony, J. E.; Malliaras, G. G. *J. Am. Chem. Soc.* **2007**, *129*, 9144.
(146) Mei, J.; Graham, K. R.; Stalder, R.; Reynolds, J. R. *Org. Lett.* **2010**, *12*, 660.
(147) Zhao, X.; Piliego, C.; Kim, B.; Poulsen, D. A.; Ma, B.; Unruh, D. A.; Fréchet, J. M. J. *Chem. Mater.* **2010**, *22*, 2325.
(148) Ajayaghosh, A. *Acc. Chem. Res.* **2005**, *38*, 449.
(149) Silvestri, F.; Irwin, M. D.; Beverina, L.; Facchetti, A.; Pagani, G. A.; Marks, T. J. *J. Am. Chem. Soc.* **2008**, *130*, 17640.
(150) Bagnis, D.; Beverina, L.; Huang, H.; Silvestri, F.; Yao, Y.; Yan, H.; Pagani, G. A.; Marks, T. J.; Facchetti, A. *J. Am. Chem. Soc.* **2010**, *132*, 4074.
(151) Wei, G.; Wang, S.; Renshaw, K.; Thompson, M. E.; Forrest, S. R. *ACS Nano* **2010**, *4*, 1927.
(152) Walker, B.; Kim, C.; Nguyen, T.-Q. *Chem. Mater.* **2011**, *23*, 470.
(153) Shang, H.; Fan, H.; Liu, Y.; Hu, W.; Li, Y.; Zhan, X. *Adv. Mater.* **2011**, *23*, 1554.
(154) Liu, Y.; Wan, X.; Wang, F.; Zhou, J.; Long, G.; Tian, J.; You, J.; Yang, Y.; Chen, Y. *Adv. Energy Mater.* **2011**, *1*, 771.
(155) Jones, B. A.; Facchetti, A.; Wasielewski, M. R.; Marks, T. J. *J. Am. Chem. Soc.* **2007**, *129*, 15259.
(156) Wang, Z.; Kim, C.; Facchetti, A.; Marks, T. J. *J. Am. Chem. Soc.* **2007**, *129*, 13362.
(157) Usta, H.; Risko, C.; Wang, Z.; Huang, H.; Deliomeroglu, M. K.; Zhukhovitskiy, A.; Facchetti, A.; Marks, T. J. *J. Am. Chem. Soc.* **2009**, *131*, 5586.
(158) Ortiz, R. O. P.; Herrera, H.; Blanco, R. L.; Huang, H.; Facchetti, A.; Marks, T. J.; Zheng, Y.; Segura, J. L. *J. Am. Chem. Soc.* **2010**, *132*, 8440.
(159) Yoon, M.-H.; Facchetti, A.; Stern, C. E.; Marks, T. J. *J. Am. Chem. Soc.* **2006**, *128*, 5792.
(160) Letizia, J. A.; Facchetti, A.; Stern, C. L.; Ratner, M. A.; Marks, T. J. *J. Am. Chem. Soc.* **2005**, *127*, 13476.
(161) Yoon, M.-H.; DiBenedetto, S. A.; Facchetti, A.; Marks, T. J. *J. Am. Chem. Soc.* **2005**, *127*, 1348.
(162) Facchetti, A.; Yoon, M.-H.; Stern, C. L.; Hutchison, G. R.; Ratner, M. A.; Marks, T. J. *J. Am. Chem. Soc.* **2004**, *126*, 13480.
(163) Facchetti, A.; Mushrush, M.; Yoon, M.-H.; Hutchison, G. R.; Ratner, M. A.; Marks, T. J. *J. Am. Chem. Soc.* **2004**, *126*, 13859.
(164) Molinari, A. S.; Alves, H.; Chen, Z.; Facchetti, A.; Morpurgo, A. F. *J. Am. Chem. Soc.* **2009**, *131*, 2462.
(165) Handa, S.; Miyazaki, E.; Takimiya, K.; Kunugi, Y. *J. Am. Chem. Soc.* **2007**, *129*, 11684.
(166) Usta, H.; Facchetti, A.; Marks, T. J. *Acc. Chem. Res.* **2011**, *44*, 501.
(167) Rivnay, J.; Jimison, L. H.; Northrup, J. E.; Toney, M. F.; Noriega, R.; Lu, S.; Marks, T. J.; Facchetti, A.; Salleo, A. *Nat. Mater.* **2009**, *8*, 952.
(168) Hau, S. K.; Cheng, Y.-J.; Yip, H.-L.; Zhang, Y.; Ma, H.; Jen, A. K. Y. *ACS Appl. Mater. Interfaces* **2010**, *2*, 1892.
(169) He, Y.; Chen, H.-Y.; Hou, J.; Li, Y. *J. Am. Chem. Soc.* **2010**, *132*, 1377.
(170) Yang, C.; Kim, J. Y.; Cho, S.; Lee, J. K.; Heeger, A. J.; Wudl, F. *J. Am. Chem. Soc.* **2008**, *130*, 6444.
(171) Backer, S. A.; Sivula, K.; Kavulak, D. F.; Fréchet, J. M. J. *Chem. Mater.* **2007**, *19*, 2927.
(172) Varotto, A.; Treat, N. D.; Jo, J.; Shuttle, C. G.; Batara, N. A.; Brunetti, F. G.; Seo, J. H.; Chabinyc, M. L.; Hawker, C. J.; Heeger, A. J.; Wudl, F. *Angew. Chem., Int. Ed.* **2011**, *50*, 5166.
(173) Zhao, G.; He, Y.; Li, Y. *Adv. Mater.* **2010**, *22*, 4355.
(174) Lee, J. K.; Wang, Y.-M.; Cho, S.; Wudl, F.; Heeger, A. J. *Org. Elec.* **2009**, *10*, 1223.
(175) Dittmer, J. J.; Marseglia, E. A.; Friend, R. H. *Adv. Mater.* **2000**, *12*, 1270.
(176) Shin, W. S.; Jeong, H.-H.; Kim, M.-K.; Jin, S.-H.; Kim, M.-R.; Lee, J.-K.; Lee, J. W.; Gal, Y.-S. *J. Mater. Chem.* **2006**, *16*, 384.
(177) Li, J.; Dierschke, F.; Wu, J.; Grimsdale, A. C.; Müllen, K. *J. Mater. Chem.* **2006**, *16*, 96.
(178) Zhan, X.; Facchetti, A.; Barlow, S.; Marks, T. J.; Ratner, M. A.; Wasielewski, M. R.; Marder, S. R. *Adv. Mater.* **2011**, *23*, 268.
(179) Kietzke, T.; Shin, R. Y. C.; Egbe, D. A. M.; Chen, Z.-K.; Sellinger, A. *Macromolecules* **2007**, *40*, 4424.
(180) Inal, S.; Schubert, M.; Sellinger, A.; Neher, D. *J. Phys. Chem. Lett.* **2010**, *1*, 982.
(181) Woo, C. H.; Holcombe, T. W.; Unruh, D. A.; Sellinger, A.; Fréchet, J. M. J. *Chem. Mater.* **2010**, *22*, 1673.
(182) Shin, R. Y. C.; Sonar, P.; Siew, P. S.; Chen, Z.-K.; Sellinger, A. *J. Org. Chem.* **2009**, *74*, 3293.
(183) Shin, R. Y. C.; Kietzke, T.; Sudhakar, S.; Dodabalapur, A.; Chen, Z.-K.; Sellinger, A. *Chem. Mater.* **2007**, *19*, 1892.
(184) Schubert, M.; Yin, C.; Castellani, M.; Bange, S.; Tam, T. L.; Sellinger, A.; Horhold, H.-H.; Kietzke, T.; Neher, D. *J. Chem. Phys.* **2009**, *130*, 094703.

(185) Ooi, Z. E.; Tam, T. L.; Shin, R. Y. C.; Chen, Z. K.; Kietzke, T.; Sellinger, A.; Baumgarten, M.; Müllen, K.; deMello, J. C. *J. Mater. Chem.* **2008**, *18*, 4619.
(186) Lim, Y.-F.; Shu, Y.; Parkin, S. R.; Anthony, J. E.; Malliaras, G. G. *J. Mater. Chem.* **2009**, *19*, 3049.
(187) Anthony, J. E. *Chem. Mater.* **2011**, *23*, 583.
(188) Shu, Y.; Lim, Y.-F.; Li, Z.; Purushothaman, B.; Hallani, R.; Kim, J. E.; Parkin, S. R.; Malliaras, G. G.; Anthony, J. E. *Chem. Sci.* **2011**, *2*, 363.
(189) Brédas, J.-L.; Norton, J. E.; Cornil, J.; Coropceanu, V. *Acc. Chem. Res.* **2009**, *42*, 1691.
(190) Brunetti, F. G.; Gong, X.; Tong, M.; Heeger, A. J.; Fred, W. *Angew. Chem., Int. Ed.* **2010**, *49*, 532.
(191) Gong, X.; Tong, M.; Brunetti, F. G.; Seo, J.; Sun, Y.; Moses, D.; Wudl, F.; Heeger, A. J. *Adv. Mater.* **2011**, *23*, 2272.
(192) Zhou, T.; Jia, T.; Kang, B.; Li, F.; Fahlman, M.; Wang, Y. *Adv. Energy Mater.* **2011**, *1*, 431.
(193) Huynh, W. U.; Dittmer, J. J.; Alivisatos, A. P. *Science* **2002**, *295*, 2425.
(194) Liu, J.; Tanaka, T.; Sivula, K.; Alivisatos, A. P.; Fréchet, J. M. J. *J. Am. Chem. Soc.* **2004**, *126*, 6550.
(195) Sun, B.; Greenham, N. C. *Phys. Chem. Chem. Phys.* **2006**, *8*, 3557.
(196) Han, L.; Qin, D.; Jiang, X.; Liu, Y.; Wang, L.; Chen, J.; Cao, Y. *Nanotechnology* **2006**, *17*, 4736.
(197) Gur, I.; Fromer, N. A.; Chen, C.-P.; Kanaras, A. G.; Alivisatos, A. P. *Nano Lett.* **2006**, *7*, 409.
(198) Lin, Y.-Y.; Chu, T.-H.; Li, S.-S.; Chuang, C.-H.; Chang, C.-H.; Su, W.-F.; Chang, C.-P.; Chu, M.-W.; Chen, C.-W. *J. Am. Chem. Soc.* **2009**, *131*, 3644.
(199) Beek, W. J. E.; Wienk, M. M.; Janssen, R. A. J. *Adv. Funct. Mater.* **2006**, *16*, 1112.
(200) Zhou, Y.; Li, Y.; Zhong, H.; Hou, J.; Ding, Y.; Yang, C.; Li, Y. *Nanotechnology* **2006**, *17*, 4041.
(201) Sun, B.; Marx, E.; Greenham, N. C. *Nano Lett.* **2003**, *3*, 961.
(202) Sun, B.; Snaith, H. J.; Dhoot, A. S.; Westenhoff, S.; Greenham, N. C. *J. Appl. Phys.* **2005**, *97*, 014914.
(203) Wang, P.; Abrusci, A.; Wong, H. M. P.; Svensson, M.; Andersson, M. R.; Greenham, N. C. *Nano Lett.* **2006**, *6*, 1789.
(204) Dayal, S.; Kopidakis, N.; Olson, D. C.; Ginley, D. S.; Rumbles, G. *Nano Lett.* **2009**, *10*, 239.
(205) Coakley, K. M.; McGehee, M. D. *Chem. Mater.* **2004**, *16*, 4533.
(206) McGehee, M. D. *MRS Bull.* **2009**, *34*, 95.
(207) Chang, J. A.; Rhee, J. H.; Im, S. H.; Lee, Y. H.; Kim, H.-j.; Seok, S. I.; Nazeeruddin, M. K.; Gratzel, M. *Nano Lett.* **2010**, *10*, 2609.
(208) Mishra, A.; Fischer, M. K. R.; Bäuerle, P. *Angew. Chem., Int. Ed.* **2009**, *48*, 2474.
(209) Hagfeldt, A.; Boschloo, G.; Sun, L.; Kloo, L.; Pettersson, H. *Chem. Rev.* **2010**, *110*, 6595.
(210) Cai, N.; Moon, S.-J.; Cevey-Ha, L.; Moehl, T.; Humphry-Baker, R.; Wang, P.; Zakeeruddin, S. M.; Gratzel, M. *Nano Lett.* **2011**, *11*, 1452.
(211) Wang, E.; Wang, L.; Lan, L.; Luo, C.; Zhuang, W.; Peng, J.; Cao, Y. *Appl. Phys. Lett.* **2008**, *92*, 033307.
(212) Scharber, M. C.; Mühlbacher, D.; Koppe, M.; Denk, P.; Waldauf, C.; Heeger, A. J.; Brabec, C. J. *Adv. Mater.* **2006**, *18*, 789.
(213) Veldman, D.; Meskers, S. C. J.; Janssen, R. A. J. *Adv. Funct. Mater.* **2009**, *19*, 1939.
(214) Gadisa, A.; Svensson, M.; Andersson, M. R.; Inganäs, O. *Appl. Phys. Lett.* **2004**, *84*, 1609.
(215) Brabec, C. J.; Cravino, A.; Meissner, D.; Sariciftci, N. S.; Fromherz, T.; Rispens, M. T.; Sanchez, L.; Hummelen, J. C. *Adv. Funct. Mater.* **2001**, *11*, 374.
(216) Perez, M. D.; Borek, C.; Forrest, S. R.; Thompson, M. E. *J. Am. Chem. Soc.* **2009**, *131*, 9281.
(217) Stevens, D. M.; Qin, Y.; Hillmyer, M. A.; Frisbie, C. D. *J. Phys. Chem. C* **2009**, *113*, 11408.
(218) Vandewal, K.; Tvingstedt, K.; Gadisa, A.; Inganäs, O.; Manca, J. V. *Nat. Mater.* **2009**, *8*, 904.
(219) Piersimoni, F.; Chambon, S.; Vandewal, K.; Mens, R.; Boonen, T.; Gadisa, A.; Izquierdo, M.; Filippone, S.; Ruttens, B.; D'Haen, J.; Martin, N.; Lutsen, L.; Vanderzande, D.; Adriaensens, P.; Manca, J. V. *J. Phys. Chem. C* **2011**, *115*, 10873.
(220) Kinoshita, Y.; Takenaka, R.; Murata, H. *Appl. Phys. Lett.* **2008**, *92*, 243309.
(221) Subbiah, J.; Kim, D. Y.; Hartel, M.; So, F. *Appl. Phys. Lett.* **2010**, *96*, 063303.
(222) Hsieh, C.-H.; Cheng, Y.-J.; Li, P.-J.; Chen, C.-H.; Dubosc, M.; Liang, R.-M.; Hsu, C.-S. *J. Am. Chem. Soc.* **2010**, *132*, 4887.
(223) Treat, N. D.; Campos, L. M.; Dimitriou, M. D.; Ma, B.; Chabinyc, M. L.; Hawker, C. J. *Adv. Mater.* **2010**, *22*, 4982.
(224) Yang, L.; Zhou, H.; You, W. *J. Phys. Chem. C* **2010**, *114*, 16793.
(225) Lee, J.-Y.; Choi, M.-H.; Song, H.-J.; Moon, D.-K. *J. Polym. Sci. Part A: Polym. Chem.* **2010**, *48*, 4875.
(226) Shockley, W.; Queisser, H. J. *J. Appl. Phys.* **1961**, *32*, 510.
(227) Veldman, D.; Ipek, O.; Meskers, S. C. J.; Sweelssen, J.; Koetse, M. M.; Veenstra, S. C.; Kroon, J. M.; van Bavel, S. S.; Loos, J.; Janssen, R. A. J. *J. Am. Chem. Soc.* **2008**, *130*, 7721.
(228) Vandewal, K.; Gadisa, A.; Oosterbaan, W. D.; Bertho, S.; Banishoeib, F.; Van Severen, I.; Lutsen, L.; Cleij, T. J.; Vanderzande, D.; Manca, J. V. *Adv. Funct. Mater.* **2008**, *18*, 2064.
(229) Tvingstedt, K.; Vandewal, K.; Gadisa, A.; Zhang, F.; Manca, J.; Inganäs, O. *J. Am. Chem. Soc.* **2009**, *131*, 11819.
(230) Vandewal, K.; Tvingstedt, K.; Gadisa, A.; Inganäs, O.; Manca, J. V. *Phys. Rev. B* **2010**, *81*, 125204.
(231) Vandewal, K.; Tvingstedt, K.; Manca, J. V.; Inganäs, O. *IEEE J. Sel. Top. Quantum Electronics* **2010**, *16*, 1676.
(232) Persson, N.-K.; Inganäs, O. *Organic Photovoltaics*; Taylor & Francis: New York, 2005.
(233) Slooff, L. H.; Veenstra, S. C.; Kroon, J. M.; Moet, D. J. D.; Sweelssen, J.; Koetse, M. M. *Appl. Phys. Lett.* **2007**, *90*, 143506.
(234) Dennler, G.; Forberich, K.; Scharber, M. C.; Brabec, C. J.; Tomis, I.; Hingerl, K.; Fromherz, T. *J. Appl. Phys.* **2007**, *102*, 054516.
(235) Burkhard, G. F.; Hoke, E. T.; McGehee, M. D. *Adv. Mater.* **2010**, *22*, 3293.
(236) Gilot, J.; Wienk, M. M.; Janssen, R. A. J. *Adv. Mater.* **2010**, *22*, E67.
(237) Kim, J. Y.; Lee, K.; Coates, N. E.; Moses, D.; Nguyen, T.-Q.; Dante, M.; Heeger, A. J. *Science* **2007**, *317*, 222.
(238) Hadipour, A.; de Boer, B.; Wildeman, J.; Kooistra, F. B.; Hummelen, J. C.; Turbiez, M. G. R.; Wienk, M. M.; Janssen, R. A. J.; Blom, P. W. M. *Adv. Funct. Mater.* **2006**, *16*, 1897.
(239) Sista, S.; Park, M.-H.; Hong, Z.; Wu, Y.; Hou, J.; Kwan, W. L.; Li, G.; Yang, Y. *Adv. Mater.* **2010**, *22*, 380.
(240) Sista, S.; Hong, Z.; Chen, L.-M.; Yang, Y. *Energy Environ. Sci.* **2011**, *4*, 1606.
(241) Ameri, T.; Dennler, G.; Lungenschmied, C.; Brabec, C. J. *Energy Environ. Sci.* **2009**, *2*, 347.
(242) Yang, J.; Zhu, R.; Hong, Z.; He, Y.; Kumar, A.; Li, Y.; Yang, Y. *Adv. Mater.* **2011**, *23*, 3465.
(243) Dennler, G.; Scharber, M. C.; Ameri, T.; Denk, P.; Forberich, K.; Waldauf, C.; Brabec, C. J. *Adv. Mater.* **2008**, *20*, 579.
(244) Wang, D. H.; Kim, D. Y.; Choi, K. W.; Seo, J. H.; Im, S. H.; Park, J. H.; Park, O. O.; Heeger, A. J. *Angew. Chem., Int. Ed.* **2011**, *50*, 5519.
(245) Salleo, A.; Kline, R. J.; DeLongchamp, D. M.; Chabinyc, M. L. *Adv. Mater.* **2010**, *22*, 3812.
(246) Gevorgyan, S. A.; et al. *Sol. Energy Mater. Sol. Cells* **2011**, *95*, 1398.
(247) Lee, M. R.; Eckert, R. D.; Forberich, K.; Dennler, G.; Brabec, C. J.; Gaudiana, R. A. *Science* **2009**, *324*, 232.
(248) Thompson, B. C.; Fréchet, J. M. J. *Angew. Chem., Int. Ed.* **2008**, *47*, 58.
(249) Gunes, S.; Neugebauer, H.; Sariciftci, N. S. *Chem. Rev.* **2007**, *107*, 1324.
(250) Chen, J.; Cao, Y. *Acc. Chem. Res.* **2009**, *42*, 1709.

(251) Bundgaard, E.; Krebs, F. C. *Sol. Energy Mater. Sol. Cells* **2007**, *91*, 954.
(252) Boudreault, P.-L. T.; Najari, A.; Leclerc, M. *Chem. Mater.* **2011**, *23*, 456.
(253) Li, C.; Liu, M.; Pschirer, N. G.; Baumgarten, M.; Müllen, K. *Chem. Rev.* **2010**, *110*, 6817.
(254) Anthony, J. E.; Facchetti, A.; Heeney, M.; Marder, S. R.; Zhan, X. *Adv. Mater.* **2010**, *22*, 3876.
(255) Gendron, D.; Leclerc, M. *Energy Environ. Sci.* **2011**, *4*, 1225.
(256) Brunetti, F. G.; Kumar, R.; Wudl, F. *J. Mater. Chem.* **2010**, *20*, 2934.
(257) Facchetti, A. *Chem. Mater.* **2010**, *23*, 733.
(258) Brabec, C. J.; Heeney, M.; McCulloch, I.; Nelson, J. *Chem. Soc. Rev.* **2011**, *40*, 1185.
(259) Hains, A. W.; Liang, Z.; Woodhouse, M. A.; Gregg, B. A. *Chem. Rev.* **2010**, *110*, 6689.
(260) Arias, A. C.; MacKenzie, J. D.; McCulloch, I.; Rivnay, J.; Salleo, A. *Chem. Rev.* **2010**, *110*, 3.
(261) Clarke, T. M.; Durrant, J. R. *Chem. Rev.* **2010**, *110*, 6736.
(262) Risko, C.; McGehee, M. D.; Bredas, J.-L. *Chem. Sci.* **2011**, *2*, 1200.